10-6-2016

Effect of Void Fraction on Transverse Shear Modulus of Advanced Unidirectional Composites

Jui-He Tai
University of South Florida, juihetai@mail.usf.edu

Effect of Void Fraction on Transverse Shear Modulus

of Advanced Unidirectional Composites

by

Jui-He Tai

A thesis submitted in partial fulfillment
of the requirements for the degree of
Master of Science in Materials Science and Engineering
Department of Chemical and Biomedical Engineering
College of Engineering
University of South Florida

Major Professor: Autar Kaw, Ph.D.
Ali Yalcin, Ph.D.
Alex Volinsky, Ph.D.

Date of Approval:
September 22, 2016

Keywords: void content, design of experiments,
finite element modeling, elastic moduli

DEDICATION

I would like to express gratitude to several people, who made enormous contributions directly or indirectly to my thesis by spending their valuable time and energy. It was my great honor to get help during my thesis work from these people. Without them, it would have been difficult to complete this thesis.

I would like to thank Professor Autar Kaw, my major advisor and professor. I benefited enormously from his advice, both for my academic and my personal life. In this research, he reinforced my gaps in knowledge in mechanical engineering, since my major was Materials Science as an undergraduate. He guided me in understanding how and why to do the research step-by-step, like telling a story and not jump around. He taught me the ways how and the reasons why to present the research writing in a fluent and coherent manner. I am so glad to have had an advisor like him in my life.

I am so fortunate to have best friends supporting me whenever I met with some difficulties. I would like to thank my friend, Swamy Rakesh Adapa. He trained me in the concepts of finite element analysis and programs like ANSYS from scratch. Moreover, he gave me many useful suggestions when I was facing some problems on the ANSYS program. Moreover, I also want to dedicate my thesis to my friends, Alexander Fyffe and Liao Kai. They gave me advice on writing and assisted me with the operations of the Minitab program.

Last, and the most important, I would like to thank my family and my girlfriend for their love. They are the most important people in my life. I would especially thank my family for their unconditional support while studying abroad in USA to pursue my dreams.

ACKNOWLEDGMENTS

I would like to express my gratitude to ANSYS, Inc. for giving permission to use ANSYS screen shots from ANSYS 17.0 academic version, and for short excerpts from documentation in ANSYS Mechanical APDL Element Reference.

I would like to express my gratitude to Minitab, Inc. for giving permission to use Minitab screen shots, and short excerpts from Minitab 15.

I would like to express my gratitude to the publishers of the Composite Science and Technology journal for giving permission to use figures from the article, “Effects of void geometry on elastic properties of unidirectional fiber reinforced composites” by Hansong Huang and Ramesh Talreja.

I would like to express my gratitude to publishers, Taylor and Francis for giving permission for using figures from the book, “Phase Transformations in Metals and Alloys”, Third Edition (Revised Reprint) by David A. Porter, et al.

TABLE OF CONTENTS

LIST OF TABLES

LIST OF FIGURES

ABSTRACT

In composite materials, transverse shear modulus is a critical moduli parameter for designing complex composite structures. For dependable mathematical modeling of mechanical behavior of composite materials, an accurate estimate of the moduli parameters is critically important as opposed to estimates of strength parameters where underestimation may lead to a non-optimal design but still would give one a safe one.

Although there are mechanical and empirical models available to find transverse shear modulus, they are based on many assumptions. In this work, the model is based on a three-dimensional elastic finite element analysis with multiple cells. To find the shear modulus, appropriate boundary conditions are applied to a three-dimensional representative volume element (RVE). To improve the accuracy of the model, multiple cells of the RVE are used and the value of the transverse shear modulus is calculated by an extrapolation technique that represents a large number of cells.

Comparing the available analytical and empirical models to the finite element model from this work shows that for polymeric matrix composites, the estimate of the transverse shear modulus by Halpin-Tsai model had high credibility for lower fiber volume fractions; the Mori-Tanaka model was most accurate for the mid-range fiber volume fractions; and the Elasticity Approach model was most accurate for high fiber volume fractions.

Since real-life composites have voids, this study investigated the effect of void fraction on the transverse shear modulus through design of experiment (DOE) statistical analysis. Fiber volume fraction and fiber-to-matrix Young’s moduli ratio were the other influencing parameters

used. The results indicate that the fiber volume fraction is the most dominating of the three variables, making up to 96% contribution to the transverse shear modulus. The void content and fiber-to-matrix Young's moduli ratio have negligible effects.

To find how voids themselves influence the shear modulus, the transverse shear modulus was normalized with the corresponding shear modulus with a perfect composite with no voids. As expected, the void content has the largest contribution to the normalized shear modulus of 80%. The fiber volume fraction contributed 12%, and the fiber-to-matrix Young's moduli ratio contribution was again low.

Based on the results of this work, the influences and sensitivities of void content have helped in the development of accurate models for transverse shear modulus, and let us confidently study the influence of fiber-to-matrix Young's moduli ratio, fiber volume fraction and void content on its value.

CHAPTER 1 LITERATURE REVIEW

1.1 Introduction

Linear elasticity mathematical models are derived using equilibrium, stress-strain, and strain-displacement equations. To solve such mathematical models, one needs to have accurate estimates of stiffness parameters. For an ideal three-dimensional material following Hooke's Law – the stress-strain relationship (Kaw, 2005) in the 1-2-3 orthogonal Cartesian coordination system is given by

$$\begin{bmatrix} \sigma_1 \\ \sigma_2 \\ \sigma_3 \\ \tau_{23} \\ \tau_{31} \\ \tau_{12} \end{bmatrix} = \begin{bmatrix} C_{11} & C_{12} & C_{13} & C_{14} & C_{15} & C_{16} \\ C_{21} & C_{22} & C_{23} & C_{24} & C_{25} & C_{26} \\ C_{31} & C_{32} & C_{33} & C_{34} & C_{35} & C_{36} \\ C_{41} & C_{42} & C_{43} & C_{44} & C_{45} & C_{46} \\ C_{51} & C_{52} & C_{53} & C_{54} & C_{55} & C_{56} \\ C_{61} & C_{62} & C_{63} & C_{64} & C_{65} & C_{66} \end{bmatrix} \begin{bmatrix} \varepsilon_1 \\ \varepsilon_2 \\ \varepsilon_3 \\ \gamma_{23} \\ \gamma_{31} \\ \gamma_{12} \end{bmatrix} \tag{1}$$

where

σ_i = normal stress in direction i, $i = 1, 2, 3$,

τ_{ij} = shear stress in plane ij, $i = 1, 2, 3, j = 1, 2, 3$,

ε_i = normal strain in direction i, $i = 1, 2, 3$,

γ_{ij} = shear strain in plane ij, $i = 1, 2, 3, j = 1, 2, 3$.

Note that *1-axis* is chosen as the direction along the fiber as shown in Figure 1.

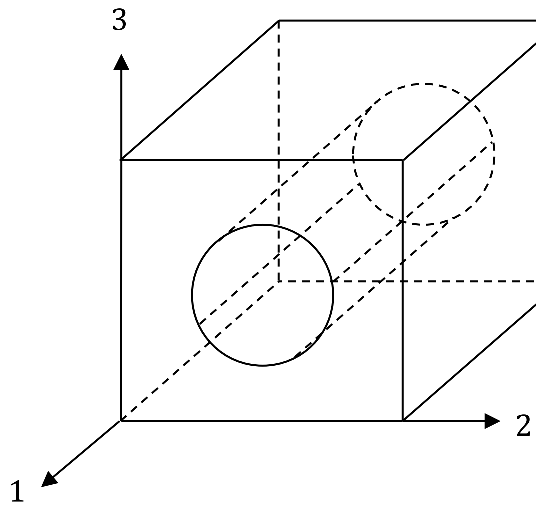

Figure 1 Definition of axes for composite models.

The 6×6 $[C]$ matrix is called the stiffness matrix. For instance, based on Equation (1), the shear stress τ_{23} can be calculated from the given formula

$$\tau_{23} = C_{41}\varepsilon_1 + C_{42}\varepsilon_2 + C_{43}\varepsilon_3 + C_{44}\gamma_{23} + C_{45}\gamma_{31} + C_{46}\gamma_{12} \tag{2}$$

Highly symmetrical geometric structure correlates to a strong similarity between mechanical behaviors in opposing directions. A typical unidirectional composite material with a matrix reinforced by long fibers can be classified as an orthotropic material. The stiffness matrix of an orthotropic material with three mutually perpendicular planes with geometric symmetry is written as (Kaw, 2005)

$$[C]_{\text{orthotropic}} = \begin{bmatrix} C_{11} & C_{12} & C_{13} & 0 & 0 & 0 \\ C_{12} & C_{22} & C_{23} & 0 & 0 & 0 \\ C_{13} & C_{23} & C_{33} & 0 & 0 & 0 \\ 0 & 0 & 0 & C_{44} & 0 & 0 \\ 0 & 0 & 0 & 0 & C_{55} & 0 \\ 0 & 0 & 0 & 0 & 0 & C_{66} \end{bmatrix} \tag{3}$$

Equation (3) of the stiffness parameters can also be written in terms of elastic moduli as

$$[C] = \begin{bmatrix} \frac{1-\nu_{23}\nu_{32}}{E_2E_3\Delta} & \frac{\nu_{21}+\nu_{23}\nu_{31}}{E_2E_3\Delta} & \frac{\nu_{31}+\nu_{21}\nu_{32}}{E_2E_3\Delta} & 0 & 0 & 0 \\ \frac{\nu_{21}+\nu_{23}\nu_{31}}{E_2E_3\Delta} & \frac{1-\nu_{13}\nu_{31}}{E_1E_3\Delta} & \frac{\nu_{32}+\nu_{12}\nu_{31}}{E_1E_3\Delta} & 0 & 0 & 0 \\ \frac{\nu_{31}+\nu_{21}\nu_{32}}{E_2E_3\Delta} & \frac{\nu_{32}+\nu_{12}\nu_{31}}{E_1E_3\Delta} & \frac{1-\nu_{12}\nu_{21}}{E_1E_2\Delta} & 0 & 0 & 0 \\ 0 & 0 & 0 & G_{23} & 0 & 0 \\ 0 & 0 & 0 & 0 & G_{31} & 0 \\ 0 & 0 & 0 & 0 & 0 & G_{12} \end{bmatrix} \tag{4}$$

where

$$\Delta = \frac{1-\nu_{12}\nu_{21}-\nu_{23}\nu_{32}-\nu_{13}\nu_{31}-2\nu_{21}\nu_{32}\nu_{13}}{E_1E_2E_3} \tag{5}$$

$E_i =$ Young's modulus in direction i, $i = 1, 2, 3$,

$\nu_{ij} =$ Poisson's ratio in plane ij, $i = 1, 2, 3, j = 1, 2, 3$.

The stiffness matrix in Equation (4) implies that for orthotropic materials, the shear strain γ_{23} is only influenced by the shear stress τ_{23}, and the slope of the linear relationship is $C_{44} = G_{23}$.

Some unidirectional composite materials such as those with symmetric periodic distribution of fibers may act as transversely isotropic material with five independent constants and is given by

$$[C]_{\text{transversely isotropic}} = \begin{bmatrix} C_{11} & C_{12} & C_{12} & 0 & 0 & 0 \\ C_{12} & C_{22} & C_{23} & 0 & 0 & 0 \\ C_{12} & C_{23} & C_{22} & 0 & 0 & 0 \\ 0 & 0 & 0 & \frac{C_{22}-C_{23}}{2} & 0 & 0 \\ 0 & 0 & 0 & 0 & C_{55} & 0 \\ 0 & 0 & 0 & 0 & 0 & C_{55} \end{bmatrix} \tag{6}$$

where the transverse shear modulus

$$G_{23} = C_{44}$$

$$= \frac{C_{22}-C_{23}}{2} \tag{7}$$

As an illustration, the stiffness matrix of an isotropic material, which has infinite symmetry planes is simplified as

$$[C]_{\text{isotropic}} = \begin{bmatrix} C_{11} & C_{12} & C_{12} & 0 & 0 & 0 \\ C_{12} & C_{11} & C_{12} & 0 & 0 & 0 \\ C_{12} & C_{12} & C_{11} & 0 & 0 & 0 \\ 0 & 0 & 0 & \dfrac{C_{11}-C_{12}}{2} & 0 & 0 \\ 0 & 0 & 0 & 0 & \dfrac{C_{11}-C_{12}}{2} & 0 \\ 0 & 0 & 0 & 0 & 0 & \dfrac{C_{11}-C_{12}}{2} \end{bmatrix} \tag{8}$$

where the two independent constants C_{11} and C_{12} in terms of elastic moduli are given by

$$C_{11} = \frac{\nu E}{(1-2\nu)(1+\nu)} \tag{9}$$

$$C_{12} = \frac{E(1-\nu)}{(1-2\nu)(1+\nu)} \tag{10}$$

where

$E =$ Young's modulus,

$\nu =$ Poisson's ratio.

In this research, we are focusing on the elastic moduli of orthotropic composite materials with square periodic arrangement of cylindrical fibers and transverse random arrangement of voids (Figure 2). In particular, we focus on the property of the transverse shear modulus. The reason to do this is as follows.

Interlaminar shear strength (ILSS) is the shear strength between the laminae in the laminate. In most cases, the value of ILSS is lower than the other mechanical properties, resulting in low overall shear strength. Also, voids are one of the common defects during laminate composite manufacturing process that considerably decreases the shear strength (Huang and Talreja, 2005). This study is hence a good start to explore the significance and the mechanism of voids effect on transverse shear modulus in composite materials to discover a better transverse shear modulus estimation method.

1.2 Predictive Models of Transverse Shear Modulus of Fiber Reinforced Composites

For a square periodic arrangement, fiber reinforced composite materials with no void fraction, various models are available to estimate the elastic moduli of composite materials. These are based on the elastic moduli and volume fractions of the fiber and matrix materials. Note that all the theories are based on the assumption that fiber and matrix materials individually are isotropic materials.

1.2.1 Voigt and Reuss Theoretical Model

Discussed by Selvadurai and Nikopour (2012), the Voigt model, also called Rule of Mixture (ROM) or iso-strain model, and the Reuss model, also called Inverse-Rule of Mixture (IROM) or iso-stress model, are the well-known simple models for evaluating elastic moduli of composite materials.

$$E_1 = E_f V_f + E_m V_m \qquad (The\ Voigt\ model) \tag{11}$$

$$\nu_{12} = \nu_f V_f + \nu_m V_m \qquad (The\ Voigt\ model) \tag{12}$$

$$\frac{1}{E_2} = \frac{V_f}{E_f} + \frac{V_m}{E_m} \qquad (The\ Reuss\ model) \tag{13}$$

$$\frac{1}{G_{12}} = \frac{V_f}{G_f} + \frac{V_m}{G_m} \qquad (The\ Reuss\ model) \tag{14}$$

where

E_1 = Longitudinal Young's modulus,

E_2 = Transverse Young's modulus,

ν_{12} = Major Poisson's ratio,

G_{12} = Axial shear modulus,

E_f = Young's modulus of fiber,

E_m = Young's modulus of matrix,

V_f = Volume fraction of fiber,

V_m = Volume fraction of matrix,

ν_f = Poisson's ratio of fiber,

ν_m = Poisson's ratio of matrix,

G_f = Shear modulus of fiber,

G_m = Shear modulus of matrix.

Also, based on the Voigt and Reuss models, the transverse shear modulus G_{23} is specified under the following inequality

$$\frac{1}{\frac{V_f}{G_f} + \frac{V_m}{G_m}} \leq G_{23} \leq G_f V_f + G_m V_m \tag{15}$$

The G_{23} calculations in this thesis would not include values obtained using Voigt and Reuss models because it only shows a range of values and not a specific value.

1.2.2 Halpin-Tsai Semi-Empirical Model

The Halpin-Tsai model is another popular model to predict elastic constants of fiber reinforced composite materials. The model is given by

$$\frac{M}{M_m} = \frac{1 + \zeta \eta V_f}{1 + \eta V_f} \tag{16}$$

$$\eta = \frac{\frac{M_f}{M_m} - 1}{\frac{M_f}{M_m} + \zeta} \tag{17}$$

where

M = Composite property,

M_f = Fiber property,

M_m =Matrix property,

ζ = Reinforcing factor.

Table 1 shows the details of how Equations (16) and (17) work (Bhalchandra, et al., 2014 and Agboola, 2011).

Table 1 Halpin-Tsai equation parameters

Composite Property (M)	Fiber Property (M_f)	Matrix Property (M_m)	Reinforcing Factor (ζ)
E_1	E_f	E_m	$2\left(\frac{L}{d}\right)$
E_2	E_f	E_m	$2, \text{when } V_f < 0.65$ $2 + 40V_f^{10}, \text{when } V_f \geq 0.65$
ν_{12}	ν_f	ν_m	$2\left(\frac{L}{d}\right)$
G_{12}	G_f	G_m	$1, \text{when } V_f < 0.65$ $1 + 40V_f^{10}, \text{when } V_f \geq 0.65$
G_{23}	G_f	G_m	$\frac{\frac{K_m}{G_m}}{\frac{K_m}{G_m} + 2} \cong \frac{1}{4 - 3\nu_m}$

where

L = the length of fiber,

d = the diameter of fiber,

K_m = the bulk modulus of matrix.

Note that when the length of fiber L is far larger than the diameter of fiber d, which implies that $\zeta \rightarrow \infty$, the equations of E_1 and ν_{12} give the formulas of the Voigt model as given by Equations (11) and (12).

1.2.3 Elasticity Approach Theoretical Model

The elasticity approach theoretical (EAP) model is the most widely used for three dimensional elastic moduli of unidirectional fiber composite. According to the study of Selvadurai and Nikopour (2012), the method is based on the relationships of three factors: force equilibrium, compatibility and Hooke's Law. The model proposed by Hashin and Rosen (1964) was initially called the composite cylinder assemblage (CCA) model, where the fibers considered are cylindrical and are in continuous periodic arrangement.

$$E_1 = E_f V_f + E_m V_m + \frac{4V_f V_m (\nu_f - \nu_m)^2}{\frac{V_f}{K_m} + \frac{V_m}{K_f} + \frac{1}{G_m}},$$

$$(The\ Hashin\ and\ Rosen\ model) \qquad (18)$$

$$\nu_{12} = \nu_f V_f + \nu_m V_m + \frac{V_f V_m (\nu_f - \nu_m)\left(\frac{1}{K_m} - \frac{1}{K_f}\right)}{\frac{V_f}{K_m} + \frac{V_m}{K_f} + \frac{1}{G_m}},$$

$$(The\ Hashin\ and\ Rosen\ model) \qquad (19)$$

$$G_{12} = \left(\frac{G_f(1 + V_f) + G_m V_m}{G_f V_m + G_m(1 + V_f)}\right) G_m,$$

$$(The\ Hashin\ and\ Rosen\ model) \qquad (20)$$

where

$$K_f = \frac{E_f}{2(1 + \nu_f)(1 - 2\nu_f)} \qquad (21)$$

$$K_m = \frac{E_m}{2(1 + \nu_m)(1 - 2\nu_m)} \qquad (22)$$

Moreover, Christensen (1990) gives the equations of the elastic moduli $G_{23}, \nu_{23},$ and E_2, based on the generalized self-consistent model given below.

$$G_{23} = \left(\frac{-B \pm \sqrt{B^2 - AC}}{A}\right) G_m, (The\ Christensen\ model) \tag{23}$$

$$\nu_{23} = \frac{K - mG_{23}}{K + mG_{23}}, (The\ Christensen\ model) \tag{24}$$

$$E_2 = 2(1 + \nu_{23})G_{23}, (The\ Christensen\ model) \tag{25}$$

where

$$A = 3V_f\left(1 + V_f\right)^2 \left(\frac{G_f}{G_m} - 1\right)\left(\frac{G_f}{G_m} + \eta_f\right) + \left[\left(\frac{G_f}{G_m} + \eta_f\right)\eta_m - \left(\frac{G_f}{G_m}\eta_m - \eta_f\right)V_f^3\right]$$
$$\left[V_f\eta_m\left(\frac{G_f}{G_m} - 1\right) - \left(\frac{G_f}{G_m}\eta_m + 1\right)\right] \tag{26}$$

$$B = -3V_f\left(1 + V_f\right)^2 \left(\frac{G_f}{G_m} - 1\right)\left(\frac{G_f}{G_m} + \eta_f\right) + \frac{1}{2}\left[\frac{G_f}{G_m}\eta_m + \left(\frac{G_f}{G_m} - 1\right)V_f + 1\right]$$
$$\left[(\eta_m - 1)\left(\frac{G_f}{G_m} + \eta_f\right) - 2\left(\frac{G_f}{G_m}\eta_m - \eta_f\right)V_f^3\right] + \frac{V_f}{2}(\eta_m + 1)\left(\frac{G_f}{G_m} - 1\right)$$
$$\left[\frac{G_f}{G_m} + \eta_f + \left(\frac{G_f}{G_m}\eta_m - \eta_f\right)V_f^3\right] \tag{27}$$

$$C = 3V_f\left(1 + V_f\right)^2 \left(\frac{G_f}{G_m} - 1\right)\left(\frac{G_f}{G_m} + \eta_f\right) + \left[\frac{G_f}{G_m}\eta_m + \left(\frac{G_f}{G_m} - 1\right)V_f + 1\right]$$
$$\left[\frac{G_f}{G_m} + \eta_f + \left(\frac{G_f}{G_m}\eta_m - \eta_f\right)V_f^3\right] \tag{28}$$

$$K = \frac{K_m\left(K_f + G_m\right)V_m + K_f(K_m + G_m)V_f}{\left(K_f + G_m\right)V_m + (K_m + G_m)V_f} \tag{29}$$

$$\eta_f = 3 - 4\nu_f \tag{30}$$

$$\eta_m = 3 - 4\nu_m \tag{31}$$

$$m = 1 + \frac{4K\nu_{12}^2}{E_1} \tag{32}$$

1.2.4 Saravanos-Chamis Theoretical Model

Saravanos and Chamis (1990) proposed a micromechanical model used commonly in aerospace industries. Based on the research from Chandra, et al. (2002), the formulas for the elastic moduli E_1 and ν_{12} are same as the Voigt model. Also, the formulas for the elastic moduli E_2 and G_{12} use $\sqrt{V_f}$ instead of V_f, and are modified. The five independent elastic moduli are rewritten as follows

$$E_1 = E_f V_f + E_m V_m \tag{33}$$

$$\nu_{12} = \nu_f V_f + \nu_m V_m \tag{34}$$

$$E_2 = \left(1 - \sqrt{V_f}\right) E_m + \frac{\sqrt{V_f} E_m}{1 - \sqrt{V_m \left(1 - \frac{E_m}{E_f}\right)}} \tag{35}$$

$$\nu_{23} = \frac{\nu_m}{1 - V_f \nu_m} + V_f \left[\nu_f - \frac{\left(1 - V_f\right)\nu_m}{1 - V_f \nu_m}\right] \tag{36}$$

$$G_{12} = \left(1 - \sqrt{V_f}\right) G_m + \frac{\sqrt{V_f} G_m}{1 - \sqrt{V_m}\left(1 - \frac{G_m}{G_f}\right)} \tag{37}$$

and

$$G_{23} = \frac{E_2}{2(1 + \nu_{23})} \tag{38}$$

1.2.5 Mori-Tanaka's Theoretical Model

Mori-Tanaka's Theoretical Model is the micromechanical model based on Eshelby's elasticity solution for unidirectional composite (Benveniste, 1987). This model assumes that there is a bridging matrix $\left[A_{ij}\right]$ which satisfies the following equation:

$$[\sigma_i^m] = \left[A_{ij}\right]\left[\sigma_j^f\right] \tag{39}$$

where

$$\left[A_{ij}\right] = \begin{bmatrix} A_{11} & A_{12} & A_{13} & 0 & 0 & 0 \\ A_{21} & A_{22} & A_{23} & 0 & 0 & 0 \\ A_{31} & A_{32} & A_{33} & 0 & 0 & 0 \\ 0 & 0 & 0 & A_{44} & 0 & 0 \\ 0 & 0 & 0 & 0 & A_{55} & 0 \\ 0 & 0 & 0 & 0 & 0 & A_{66} \end{bmatrix} \tag{40}$$

$\left[\sigma_i^f\right] =$ the volume averaged stress tensors of the fiber,

$[\sigma_i^m] =$ volume averaged stress tensors of the matrix.

In the bridging matrix $\left[A_{ij}\right]$, the formula of all the entries are derived as

$$A_{11} = \frac{E_m}{E_f}\left[1 + \frac{(\nu_f - \nu_m)\nu_m}{(\nu_m + 1)(\nu_m - 1)}\right] \tag{41}$$

$$A_{12} = A_{13}$$

$$= \frac{E_m}{E_f}\left(\frac{(\nu_f - 1)\nu_m}{2(\nu_m + 1)(\nu_m - 1)} + \frac{\nu_f}{(\nu_m + 1)(\nu_m - 1)}\right) - \frac{\nu_m}{2(\nu_m - 1)} \tag{42}$$

$$A_{21} = A_{31}$$

$$= \frac{E_m}{E_f}\frac{\nu_f - \nu_m}{2(\nu_m + 1)(\nu_m - 1)} \tag{43}$$

$$A_{22} = A_{33}$$

$$= \frac{E_m}{E_f}\left[\frac{\nu_f - 3}{8(\nu_m + 1)(\nu_m - 1)} + \frac{\nu_f\nu_m}{2(\nu_m + 1)(\nu_m - 1)}\right]$$

$$+ \frac{(\nu_m + 1)(4\nu_m - 5)}{8(\nu_m + 1)(\nu_m - 1)} \tag{44}$$

$$A_{23} = A_{32}$$

$$= \frac{E_m}{E_f}\left[\frac{3\nu_f - 1}{8(\nu_m - 1)(\nu_m + 1)} + \frac{\nu_f\nu_m}{2(\nu_m - 1)(\nu_m + 1)}\right]$$

$$- \frac{(\nu_m + 1)(4\nu_m - 1)}{8(\nu_m + 1)(\nu_m - 1)} \tag{45}$$

$$A_{44} = \frac{G_m}{G_f}\frac{-1}{4(\nu_m - 1)} + \frac{4\nu_m - 3}{4(\nu_m - 1)} \quad (46)$$

$$A_{55} = A_{66}$$

$$= \frac{G_f + G_m}{2G_f} \quad (47)$$

Mori-Tanaka's model results in the following formulae

$$E_1 = \frac{k_1 + E_m k_2 + E_f E_m V_f^2}{k_2 + k_3 + E_m V_f^2} \quad (48)$$

$$E_2 = \frac{k_1\left[V_f + V_m(A_{22} + A_{32})\right] + E_m k_2 + E_f E_m V_f^2}{k_5 + \left(E_f E_m b_5 + E_f V_m^2 A_{22}^2\right)\left(V_f + V_m A_{11}\right)} \quad (49)$$

$$\nu_{12} = \frac{k_2 \nu_m + k_4 + E_m \nu_f V_f^2}{k_2 + k_3 + E_m V_f^2} \quad (50)$$

$$G_{12} = \frac{G_f G_m\left(V_f + V_m A_{66}\right)}{G_m V_f + G_f V_m A_{66}} \quad (51)$$

$$G_{23} = \frac{G_f G_m\left(V_f + V_m A_{44}\right)}{G_m V_f + G_f V_m A_{44}} \quad (52)$$

where

$$k_1 = E_f E_m V_f V_m (A_{11} + A_{22} + A_{32}) \quad (53)$$

$$k_2 = E_f V_m^2 [A_{11}(A_{22} + A_{32}) - 2A_{12}A_{21}] \quad (54)$$

$$k_3 = V_f V_m\left[2A_{21}\left(E_m \nu_f - E_f \nu_m\right) + E_m(A_{22} + A_{32}) + E_f A_{11}\right] \quad (55)$$

$$k_4 = V_f V_m\left[A_{12}\left(E_m - E_f\right) + E_f \nu_m (A_{22} + A_{32}) + A_{11} E_m \nu_f\right] \quad (56)$$

$$k_5 = E_f E_m V_m [A_{22}(b_1 + b_2) + A_{12}(b_3 + b_4)] \quad (57)$$

1.2.6 Bridging Theoretical Model

The bridging micromechanical model was proposed by Huang (2000, 2001). According to Liu and Huang (2014), similar to Mori-Tanaka's model, Bridging Theoretical Model also assumes that there is a bridging matrix $[A_{ij}]$ which satisfies the following equation:

$$[\sigma_i^m] = [A_{ij}][\sigma_j^f] \tag{39}$$

where

$[\sigma_i^f] =$ the volume averaged stress tensors of the fiber,

$[\sigma_i^m] =$ volume averaged stress tensors of the matrix.

However, the difference between the two theories is that they have different opinions on the symmetry of their model and numbers of independent elastic constants, deriving different bridging matrix $[A_{ij}]$ on the calculation. Since the $[A_{ij}]$ matrix is different from the bridging model, the formulas of elastic moduli are different (Zhou and Huang, 2012).

$$[A_{ij}] = \begin{bmatrix} a_{11} & a_{12} & a_{13} & a_{14} & a_{15} & a_{16} \\ 0 & a_{22} & a_{23} & a_{24} & a_{25} & a_{26} \\ 0 & 0 & a_{33} & a_{34} & a_{35} & a_{36} \\ 0 & 0 & 0 & a_{44} & a_{45} & a_{46} \\ 0 & 0 & 0 & 0 & a_{55} & a_{56} \\ 0 & 0 & 0 & 0 & 0 & a_{66} \end{bmatrix} \tag{58}$$

With the bridging matrix $[A_{ij}]$, the elastic moduli are given by

$$E_1 = E_f V_f + E_m V_m \tag{59}$$

$$\nu_{12} = \nu_f V_f + \nu_m V_m \tag{60}$$

$$E_2 = \frac{(V_f + V_m a_{11})(V_f + V_m a_{22})}{(V_f + V_m a_{11})\left(\frac{V_f}{E_f} + \frac{V_m}{E_m} a_{22}\right) + V_f V_m \left(\frac{1}{E_m} - \frac{1}{E_f}\right) a_{12}}$$

$$= (V_f + V_m a_{11})(V_f + V_m a_{22})^2 d_3 \tag{61}$$

$$G_{12} = \frac{(V_f + V_m a_{66}) G_f G_m}{V_f G_m + V_m G_f a_{66}}$$

$$= \frac{(G_f + G_m) + V_f(G_f - G_m)}{(G_f + G_m) - V_f(G_f - G_m)} G_m \tag{62}$$

$$\nu_{23} = \frac{d_4}{d_3} \tag{63}$$

$$G_{23} = \frac{1}{2}\frac{E_2}{1+\nu_{23}}$$

$$= \frac{1}{2}\frac{V_f + V_m a_{44}}{V_f\left(\frac{1+\nu_f}{E_f}\right) + V_m\left(\frac{1+\nu_m}{E_m}\right)a_{44}} \tag{64}$$

where the entries in the bridging matrix are derived as

$$a_{11} = \frac{E_m}{E_f} \tag{65}$$

$$a_{22} = a_{33} = a_{44}$$

$$= \beta + (1-\beta)\frac{E_m}{E_f}, \tag{66}$$

$$a_{12} = \frac{\left(E_m\nu_m - E_f\nu_f\right)(a_{11} - a_{22})}{E_m - E_f} \tag{67}$$

$$a_{55} = a_{66} = \alpha + (1-\alpha)\frac{G_m}{G_f}, \tag{68}$$

where

$$0 < \alpha < 1 \ (\alpha = 0.3\sim 0.5 \ in\ most\ cases)$$

$$0 < \beta < 1 \ (\beta = 0.35\sim 0.5 \ in\ most\ cases)$$

$$d_3 = \left(\frac{V_f}{E_f} + \frac{V_m a_{22}}{E_m}\right)\left[V_f^2 + V_f V_m(a_{11} + a_{22}) + V_m^2(a_{11}a_{22})\right]$$

$$+V_f V_m a_{12}\left(V_f + V_m a_{22}\right)\left(\frac{\nu_f}{E_f} - \frac{\nu_m}{E_m}\right) \tag{69}$$

$$d_4 = V_f V_m a_{12}\left(V_f + V_m a_{22}\right)\left(\frac{\nu_m}{E_m} - \frac{\nu_f}{E_f}\right) + \frac{\nu_f}{E_f}\left[V_f^3 + V_f V_m a_{22}\left(V_f + \frac{E_m V_m}{E_f}\right)\right]$$

$$+\frac{\nu_m V_f V_m a_{22}}{E_m}\left[V_f + V_m(a_{11} + a_{22})\right] + \frac{E_m V_m}{E_f}\left(V_f^2 + V_m^2 a_{22}^2\right) \tag{70}$$

1.2.7 Whitney and Riley Theoretical Model

The Whitney and Riley Theoretical Model (Seiler, et al. 1966 and Selvadurai and Nikopour, 2012), is based on energy weighting methods, and is different from most of other theories that are based on elasticity models.

$$E_1 = V_f\left(E_f - E_m\right) + V_m E_m \tag{71}$$

$$\nu_{12} = \nu_m - \frac{2\left(\nu_m - \nu_f\right)(1-\nu_m)^2 E_f V_f}{E_m\left(1-\nu_f\right)L_f + E_f\left(V_f L_m + \nu_m + 1\right)} \tag{72}$$

$$\nu_{23} = V_f \nu_f + V_m \nu_m \tag{73}$$

$$G_{23} = \frac{\left(G_f + G_m\right) + \left(G_f - G_m\right)G_m V_f}{\left(G_f + G_m\right) - \left(G_f - G_m\right)V_f} \tag{74}$$

where

$$L_f = 1 - \nu_f - \nu_f^2 \tag{75}$$

$$L_m = 1 - \nu_m - \nu_m^2 \tag{76}$$

Note that this theory gives equations for four out of the five independent elastic moduli.

1.3 Scale Effects of Finite Domain Models

A unit cell, or so-called a representative volume element (RVE) of composite model is described as a cylindrical fiber embedded into the center of a volumetrically proportionate matrix of specific geometric shape, such as a cuboid matrix with a square cross-sectional area**.** Based on the RVE model, Finite Element Analysis method (FEA) is a credible numerical method to study mechanical properties of composite materials.

Jiang, et al. (2001) defines window size δ to standardize the domain size of FEM models by the following equation

$$\delta = \frac{L}{d_f} \geq 1 \tag{77}$$

where

L = the length of unit cell,

d_f = the diameter of fiber in the cell.

Also, the relationship window size δ between domain size D or the so-called number of cells can be written by

$$D = \delta^2 \tag{78}$$

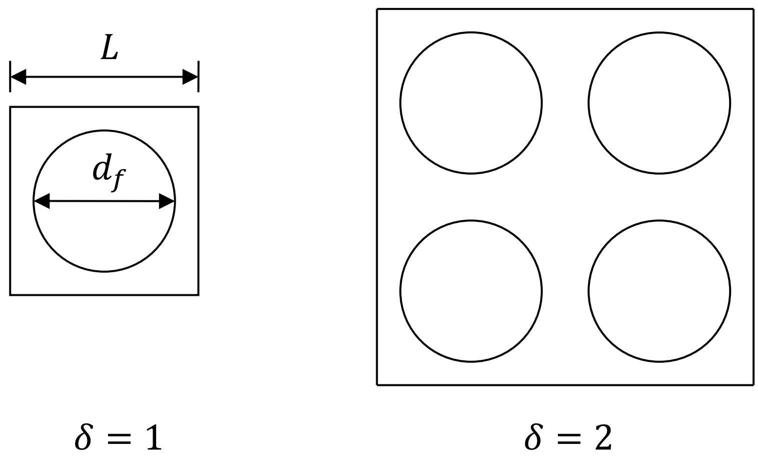

Figure 2 Window parameter δ subject to varying scales.

In this research, the impact of domain size on G_{23} value is observed, but would be normalized by the following equation

$$\frac{G_{23}}{G_m} = \alpha + \frac{\beta}{(D)^\gamma} \tag{79}$$

where α, β, and γ are constants.

Considering reality, composite products in the scale used in daily application, the value of D is large, which means the value of $\frac{\beta}{(D)^\gamma}$ would be close to zero for positive γ, resulting in the value of G_{23}/G_m converge to α, and hence call it transverse shear modulus ratio $(G_{23})_\infty/G_m$.

1.4 Voids

1.4.1 Nucleation

There is no exact and unified mechanism for voids formation. However, the most accepted and frequently mentioned mechanism for glass/epoxy and graphite/epoxy is defects induced in manufacturing processes (Hamidi, et al. 2004, 2005, and Bowles and Frimpong, 1992).

Little, et al. (2012) point out that void content is not the only factor that affects composite mechanical properties, but that size, shape and distribution of voids are significant factors that influence the mechanical response. Influenced by so many factors, gas-entraining voids produced in the mechanical mixing process result in inconsistent size, shape, and content of void.

To simplify the situation, the shape of voids are considered as spherical or cylindrical in many of theories (Bowles and Frimpong, 1992). Jena and Chaturvedi, (1992) and Porter, et al. (2009), which are two examples under cylindrical void shape assumption, have discussion of kinetics theories of nucleation. The first boundary condition of homogeneous nucleation is that it is an energy balance process between surface energy γ and volume free energy change ΔG_v. Therefore the equation of total Gibbs free energy ΔG is written as

$$\Delta G = \frac{4}{3}\pi r^3 \Delta G_v + 4\pi r^2 \gamma \tag{80}$$

where

$r =$ the radius of voids.

Also, we know that the reaction will be stopped when the system reaches steady state, where ΔG would stay at its minimum.

$$\frac{\partial \Delta G}{\partial r} = 0$$

$$= \frac{4}{3}\pi r^2 \Delta G_v + 8\pi r \gamma \tag{81}$$

In thermodynamics, the Gibbs free energy is defined as

$$\Delta G = \Delta H - T\Delta S \tag{82}$$

where

ΔH = enthalpy change of reactions,

T = current temperature of the system,

ΔS = entropy change of reactions.

Also, when $T = T_0$, where T_0 is the equilibrium transition temperature of voids, and ΔH_v is the enthalpy difference between the two phases.

$$\Delta G = \Delta H_v - T_0\Delta S = 0 \tag{83}$$

$$\Delta S = \frac{\Delta H_v}{T_0} \tag{84}$$

Assuming that $\Delta H \cong \Delta H_v$ for any temperature, we have

$$\Delta G = \Delta H_v\left(\frac{T_0 - T}{T_0}\right) \tag{85}$$

Therefore

$$\begin{aligned} r_c &= -\frac{2\gamma}{\Delta G_v} \\ &= -\frac{2\gamma}{\Delta H_v\left(\frac{T_0 - T}{T_0}\right)} \end{aligned} \tag{86}$$

$$\begin{aligned} \Delta G_{c,homo} &= \frac{16\pi\gamma^3}{3(\Delta G_v)^2} \\ &= \frac{16\pi\gamma^3}{3\left[\Delta H_v\left(\frac{T_0 - T}{T_0}\right)\right]^2} \end{aligned} \tag{87}$$

where

r_c = critical radius of void clusters,

$\Delta G_{c,homo}$ = critical free energy barrier of void clusters through homogeneous nucleation.

The total Gibbs free energy curve is shown in Figure 3, where r_c is equal to r^* in the figure. For those clusters where $r < r_c$, the surface energy is larger than the volume free energy, resulting in that the clusters are unstable, and will shrink after reaction. On the other side, for those clusters where $r > r_c$, the surface energy is smaller than the volume free energy, resulting in that the clusters are stable and have a chance to become voids.

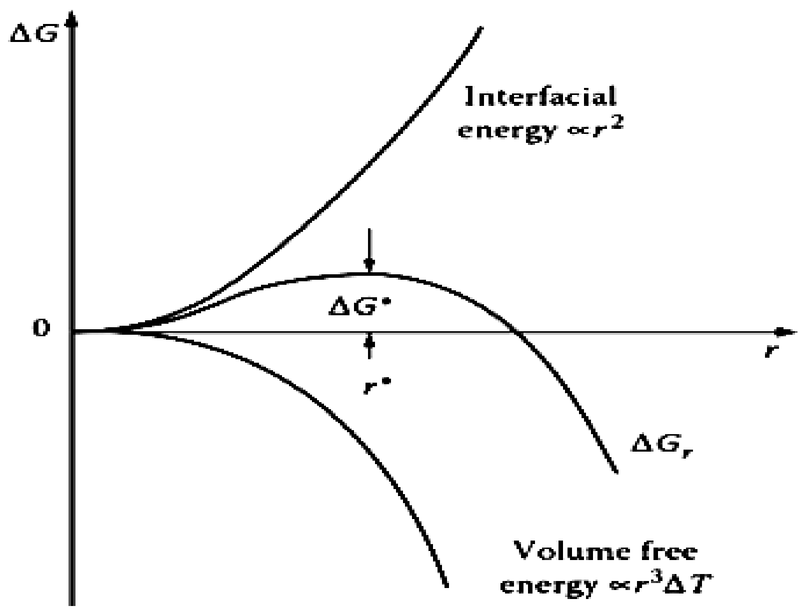

Figure 3 The free energy change associated with homogeneous nucleation of a sphere of radius (Porter, 2009).

Secondly, the Boltzmann distribution is an assumption for void distribution based on thermodynamic equilibrium, considering the void clusters are of same radius resulting from under the uniformity of the thermal environments. Because of the total free energy ΔG_c is limited, the equation is

$$N_{r_c} = N_0 exp\left(-\frac{\Delta G_c}{RT}\right) \tag{88}$$

where

N_{r_c} = the number of clusters with radius r_c per unit volume,

N_0 = the number of clusters in the system per unit volume.

Therefore, the voids volume fraction f_v can be written as

$$
\begin{aligned}
f_v &= N_{r_c}\left(\frac{4}{3}\pi r_c^3\right) \\
&= N_0\left[\frac{4}{3}\pi(r_c^3)\right] exp\left(-\frac{\Delta G_c}{RT}\right) \\
&= -\frac{4}{3}\pi N_0\left(\frac{2\gamma}{\Delta H_v\left(\frac{T_0-T}{T_0}\right)}\right)^3 exp\left\{-\frac{16\pi\gamma^3}{3RT\left[\Delta H_v\left(\frac{T_0-T}{T_0}\right)\right]^2}\right\}
\end{aligned} \tag{89}
$$

Furthermore, the homogeneous nucleation rate I can be rewritten as

$$q_0 = \frac{\alpha P}{\sqrt{2\pi MkT}} \tag{90}$$

$$O_c = 4\pi r_c^2 \tag{91}$$

$$Z_c = N_{r_c} \tag{92}$$

$$I = q_0 O_c Z_c \tag{93}$$

where

q_0 = jump frequency,

α = accommodation or sticking coefficient,

P = vapor pressure of voids,

M = average molecular mass of voids,

k = Boltzmann constant,

O_c = surface contact area of critical clusters,

Z_c = number of critical clusters.

Therefore

$$I = \left(\frac{\alpha P}{\sqrt{2\pi MkT}}\right)(4\pi r_c^2)\left[N_0 exp\left(-\frac{\Delta G_c}{RT}\right)\right]$$

$$= \frac{4\sqrt{\pi}\alpha r_c^2 N_0 P}{\sqrt{2MkT}} exp\left\{-\frac{16\pi\gamma^3}{3RT\left[\Delta H_v\left(\frac{T_0 - T}{T_0}\right)\right]^2}\right\} \quad (94)$$

Therefore, the radius, number of voids and rate of voids nucleation can be controlled by governing pressure and temperature in the manufacturing processes.

Heterogeneous nucleation occurs on impurities particles, strained regions, interface, surface defects, and broken structure, which enable clusters becoming voids with smaller free energy of activation in the same radius than homogeneous nucleation. The critical free energy of heterogeneous nucleation is given by

$$\Delta G_{c,hetro} = \Delta G_{c,homo}\left(\frac{2 - 3cos\theta + cos^3\theta}{4}\right)$$

$$= \frac{16\pi\gamma^3}{3(\Delta G_v)^2}\left(\frac{2 - 3cos\theta + cos^3\theta}{4}\right)$$

$$= \frac{4\pi\gamma^3 T_0^2(2 - 3cos\theta + cos^3\theta)}{3\Delta H_v^2(T_0 - T)^2} \quad (95)$$

where

$\Delta G_{c,hetro}$ = critical free energy barrier of void clusters through heterogeneous nucleation,

θ = contact angle of surface defect and interface between fibers and matrix.

However, the situation of homogeneous nucleation would not be considered in this research, because all the voids would be formed on the interface between fibers and matrix. To focus on the characteristic and effect of different void content, the simple model in this research is square packed arrangement fiber in matrix with cylindrical voids at random positions.

1.4.2 Volume Content

There are two possible methods to represent void content. The first method considers voids as a kind of defect structure on the matrix. In other words, it is part of the matrix. Therefore the void content f_v is volume percentage of the void volume. The equation can be written as

$$V_f + V_m^* = 1 \tag{96}$$

$$V_m^* = f_v + f_m \tag{97}$$

where

V_f = Fiber volume fraction,

V_m^* = Total matrix volume fraction,

f_m = Matrix volume fraction except the void content.

Indeed, this method seems reasonable because the method is a good way on reflecting the density of void in the matrix.

The other method is considering voids as a third material as fibers or particulates embedded into the matrix. Then

$$V_f + V_m + V_v = 1 \tag{98}$$

where

V_f = Fiber volume fraction,

V_m = Matrix volume fraction,

V_v = Voids volume fraction.

This method also seems reasonable because the method gives more specific description on voids, which is conducive on further studies of void properties.

Therefore, the research adopts the latter method to define void content as V_v, which satisfies the following relationship

$$V_f + V_m + V_v = 1 \tag{98}$$

$$V_v = \left(1 - V_f\right) \times f_v \tag{99}$$

1.4.3 Size, Shape and Distribution

Based on the derivation of nucleation by kinetic theories in Section 1.4.1, we know that void content, radius of voids, and the rate of nucleation are determined when the pressure and temperature of system are known. In fact, the relationship between voids content and radius of voids has been further discussed by Huang and Talreja (2005). Based on their work, all the models in this research are adopting a unified cylinder void shape through its length and of radius (Figure 4):

$$r_v = \frac{d_v}{2} = \frac{1}{2}\left[(1.93 \times 10^{-2}) - (1.2 \times 10^{-2}) \times e^{(-87 \times f_v)}\right] \tag{100}$$

where

r_v = the radius of voids (mm),

f_v = the void contents, defined as the ratio of volume of voids to volume of matrix and voids.

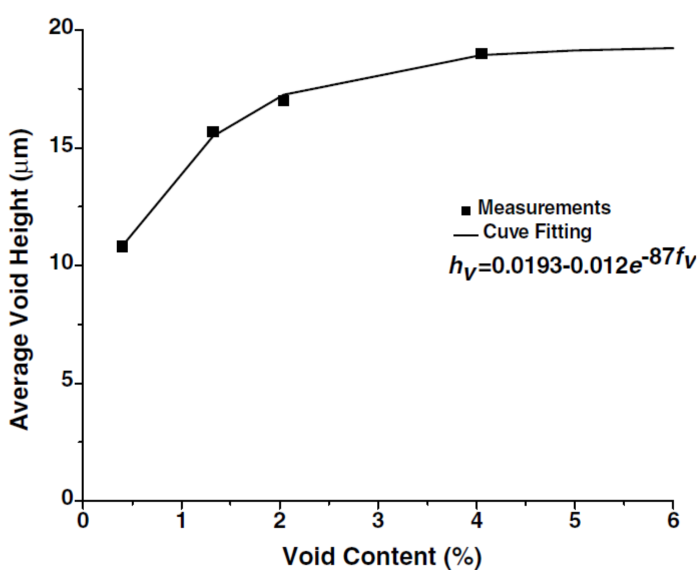

Figure 4 The average void height vs. void content (Huang and Talreja, 2009).

Although size, shape and distribution of voids are significant factors that influence the mechanical response, we are not considering the impact of voids distribution. The reason is that although different voids distribution would result in decrease of G_{23} value by different amounts, the voids positions are not controllable during manufacturing processes.

CHAPTER 2 FORMULATION

2.1 Finite Element Modeling

To determine the impact of voids on the transverse shear modulus G_{23}, matrix laboratory (MATLAB®, 2012) and ANSYS Parametric Design Language (ANSYS® APDL, 2016) programs were selected to simulate the effects of geometrical configurations, boundary conditions, fiber-to-matrix Young's moduli ratios, and fiber and void volume fractions on the model.

MATLAB, a powerful programming language capable of numerical computing, played an important role in providing randomly-generated two-dimensional coordinate points and of programming APDL codes into *.dbs files. The significant benefit of producing APDL code files via the MATLAB platform is that highly developed looping application functions make the code shorter and more logical. In other words, MATLAB simplifies the modification processes and lowers the risks of typographical errors, resulting in saving more time on testing and debugging processes.

The ANSYS APDL program is used for computing numerical simulations with finite element analysis because of its powerful capability to solve mechanical problems. In addition to being able to create models through selecting options on the user interface, users of the APDL program are also able to build models by entering custom codes. By loading the code files produced from MATLAB, we can save time and redundancy from manually entering those commands for each model.

2.2 Geometrical Design

The RVE composite model was previously discussed in Section 1.3. In this research, the local coordinate system axes of the composite model are defined by the coordinate system of $(1, 2, 3)$, which corresponds to the global coordinate system (z, x, y). The local system is defined such that the origin is located at the bottom left corner of the back face of the RVE.

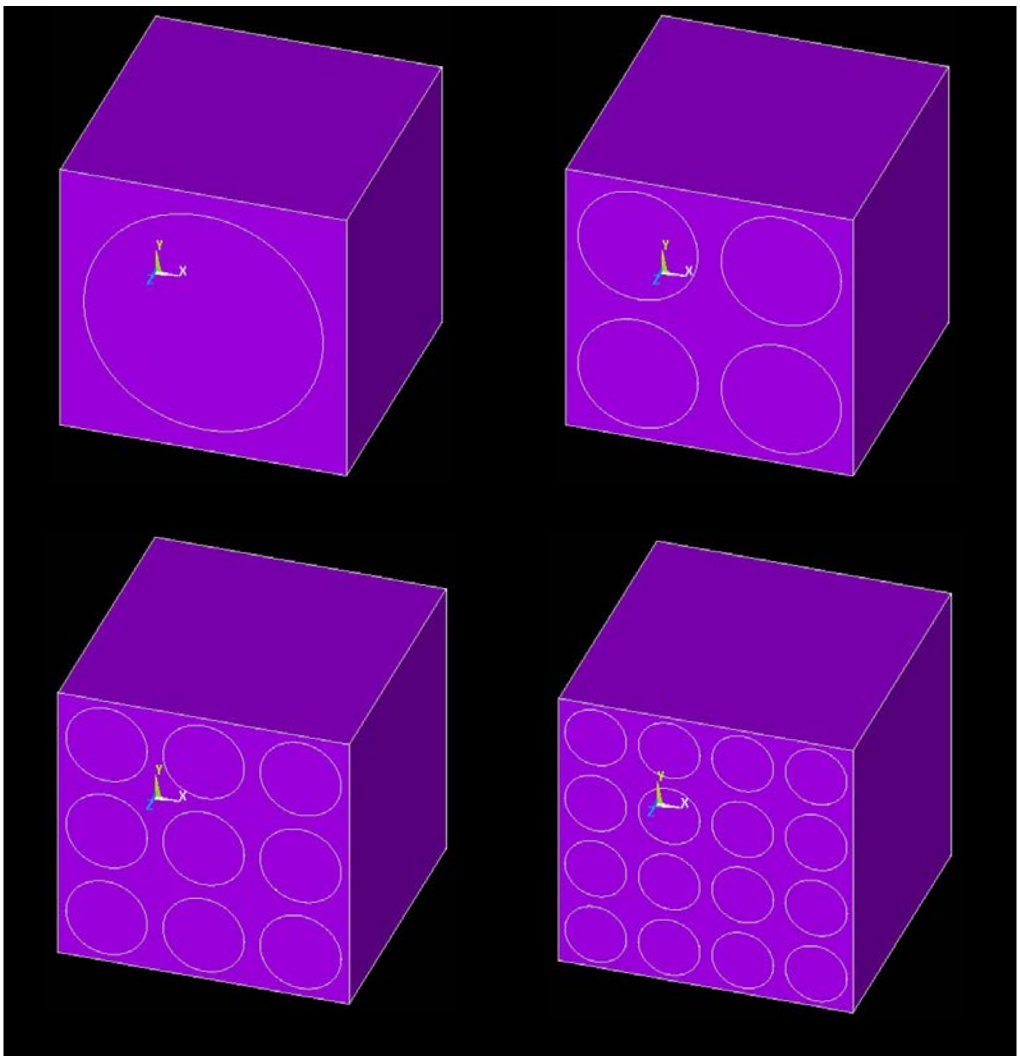

Figure 5 The model in the global coordinate system axes.

To proceed, some assumptions of mechanical behaviors have been made in order to simplify the study of the composite material. For all models, each section of RVE cells, parallel to the x-y plane, are square with side lengths of 1mm. The cylindrical fibers are embedded within the center of each cell and are extruded along the z-axis. In addition, the thickness of all models is same as their x-y face edges, therefore all models are cubic bodies.

2.2.1 Material Properties of Fibers and Matrix

Summarized from the theories discussed in Chapter 1, it has been shown that the elastic moduli of fiber and matrix play an important role in affecting the G_{23} modulus. To understand the impact of the void fraction on values of G_{23} with different material properties, we design three fiber materials with different fiber to matrix elastic moduli ratio E_f/E_m $(20, 50,\ \text{and } 80)$. These values for the different models are listed in Table 2. Therefore, the selected materials range between a low elastic moduli ratio E_f/E_m of 20 (glass/epoxy composites) to a high elastic moduli ratio of 80 (graphite/epoxy composites).

Table 2 Material properties of fibers and matrix

Material	Fiber-to-matrix Young's modulus ratio, E_f/E_m	Poisson's Ratio, ν
Fiber #20	20	0.2
Fiber #50	50	0.2
Fiber #80	80	0.2
Matrix	-	0.3

2.2.2 Variable Fiber Volume Fraction of Square Packed Array Composite

In addition to material properties, the fiber volume fraction also serves a primary role in determining the value of G_{23}. For square-packed array fiber-reinforced composites, the fiber volume fraction V_f is denoted here as a term to describe the relationship between the diameter of the fiber d and the distance between two fibers s. Formally, their relationship is defined by the following formula (Kaw, 2005)

$$\frac{d}{s} = \left(\frac{V_f}{\pi}\right)^{1/2} \tag{101}$$

Limited by geometry, this formula yields the maximum value of

$$V_f = \frac{\pi}{4}$$

$$= 78.540\% \tag{102}$$

Therefore, to portray the effects on G_{23} based on different fiber volume fractions, different percent compositions were studied. Namely, fiber volume fractions of 40%, 55% and 70% are investigated. Furthermore, because this research assumes that the edge of a unit cell s is 1mm in length, the radius of the fibers, $r_f = \frac{d}{2}$, have been calculated and are listed in Table 3.

Table 3 Radius of fibers for different fiber volume fraction ($s = 1\text{mm}$)

Fiber Volume Fraction, V_f (%)	Radius of Fiber, r_f (mm)
40	0.3568
55	0.4184
70	0.4720

2.2.3 Variable Domain Size of Square Packed Array Composite

The effect of the domain size of composite models was briefly discussed in Section 1.4. This study allows us to speculate the mechanical behavior of composites by observing the tendency of the dimensionless shear modulus ratio G_{23}/G_m value as the domain size increases. In common situations, the composite materials often used in real-world applications are far too complex, that is, they contain considerable amounts of cells. These materials are too complicated for the finite element analysis program to simulate directly. In this study, the correlation between G_{23}/G_m values and domain sizes are calculated from the following formula

$$\frac{G_{23}}{G_m} = \alpha + \frac{\beta}{(D)^{\gamma}}$$

$$= \alpha + \frac{\beta}{(\delta)^{2\gamma}} \tag{103}$$

where α, β, and γ are constants solved by substituting G_{23}/G_m values of the models with domain size δ from 1 to 4 into the Curve Fitting tool in MATLAB, where the geometry is shown in Figure 5. Upon inspection of the formula, it becomes apparent that the value of G_{23}/G_m in models containing a large number of cells will eventually converge to α as the second term of Equation (103) tends to zero, and hence call α as $(G_{23})_\infty/G_m$.

Additionally, it should be noted that the interface between fibers and the matrix is assumed to be perfectly bonded.

2.2.4 Void Design of Square Packed Array Composites

To simplify the model, some boundary conditions for voids are established. Just as the shape of the fiber is cylindrical, so too is the shape of the void, being formed from a circular section on the x-y plane which is extruded along the z-axis. According to the research done by Huang (2005), the radius of voids r_v in models can be derived by the following formula

$$V_v = \left(1 - V_f\right) \times f_v \tag{104}$$

$$r_v = (9.65 \times 10^{-6}) - (6 \times 10^{-6}) \times e^{(-87 \times f_v)} \tag{105}$$

The calculated values are shown in Table 4. The selected void content range in this study is between 0% and 3%. The research from Liu, et al. (2006) has indicated that the void content is critical on dynamic aerospace composite application, where 1% void content above is intolerable. Moreover, Ghiorse (1991) mentions that the void content of advanced dynamic aerospace structures, such as helicopters, should not be more than 1.5%. On the other side, for the applications which are not critically dependent on low void volume, high-level void content such as 5% and higher, is still acceptable (Ghiorse 1991 and Liu, et al. 2006). Examples include ground vehicle components.

Table 4 Void fraction transfer, void radius, and number of voids for different fiber volume fractions

$V_f(\%)$		40			55			70		
$V_v(\%)$		1	2	3	1	2	3	1	2	3
$f_v(\%)$		1.667	3.333	5	2.222	4.444	6.667	3.333	6.667	10
$r_v(\mu m)$		8.2430	9.3198	9.5726	8.7818	9.5244	9.6318	9.3198	9.6318	9.6490
$(\#void)$										
δ^2	1	59	73	104	41	70	103	37	69	103
	4	235	293	417	165	281	412	147	274	410
	9	528	660	938	371	632	926	330	618	923
	16	938	1173	1667	660	1123	1647	586	1098	1641

The position of voids are randomly-generated, but they must also adhere to the following stipulations. Firstly, we presume that the voids should maintain cylindrical structure in the matrix. Therefore, the distance between the void and the interface of the nearest fiber should be larger than the radius of void. This is expressed by the following inequality

$$D_{f-v} > r_f + r_v \tag{106}$$

where

D_{f-v} = distance between the void center point and the nearest fiber,

r_f = the radius of the fiber,

r_v = the radius of void.

Secondly, we assume that the voids are completely in the matrix. This means that the distance between the edge of the matrix and the center of the voids should be larger than the radius of the voids. The parametric inequalities of the center coordinates of the voids on the x-y plane are expressed by

$$r_v < x_v < L_m\delta - r_v \text{ for the range of possible } x\text{-coordinate} \tag{107}$$

$$r_v < y_v < L_m\delta - r_v \text{ for the range of possible } y\text{-coordinate} \tag{108}$$

where

x_v and $y_v =$ the x and y coordinates of the void center,

$L_m =$ length of the edge of the matrix,

$\delta =$ domain size of the model.

Finally, we specify that the voids are separate from one another, meaning that the voids will never overlap nor combine into larger voids. This condition is expressed as the inequality below

$$D_{v-v} > 2r_v \tag{109}$$

where

$D_{v-v} =$ the distance between any two void centers.

Note that before a new void is generated, the minimum distance between its coordinates and all other previous points coordinates should be examined.

To produce void coordinates which satisfy these three boundary conditions above, the first step is to create two series of uniformly distributed random numbers which both range from r_f to $L_m\delta - r_f$ expressed as x and y coordinates. Following this, the next step is to classify the points based on their distance to the nearest central coordinates of a fiber. Once this is done, the newly-generated points must be filtered by the conditions of the inequality

$$D_{f-v} > r_f + r_v \tag{110}$$

The final step is checking the distance between a probable new point and the previously plotted points.

2.3 Meshing Elements of Geometric Models

2.3.1 Bulk Elements

We use ANSYS Solid185 elements to simulate the problem. Solid185 is an 8-node, 3D element for structural or layered solids. This element type, which is shown in Figure 6, is comprised of a node on each of the eight corners which are connected by twelve straight lines. These lines, which serve as the edges of the element, can be described by linear equations. This provides a substantial improvement in the solving of these equations when compared with higher order expressions, such as quadratics. The selection of Solid185 in this research is made because this element type is commonly used due to the ease of deducing its mechanical properties concerning plasticity, stress stiffening, large deflections, and high amounts of strain.

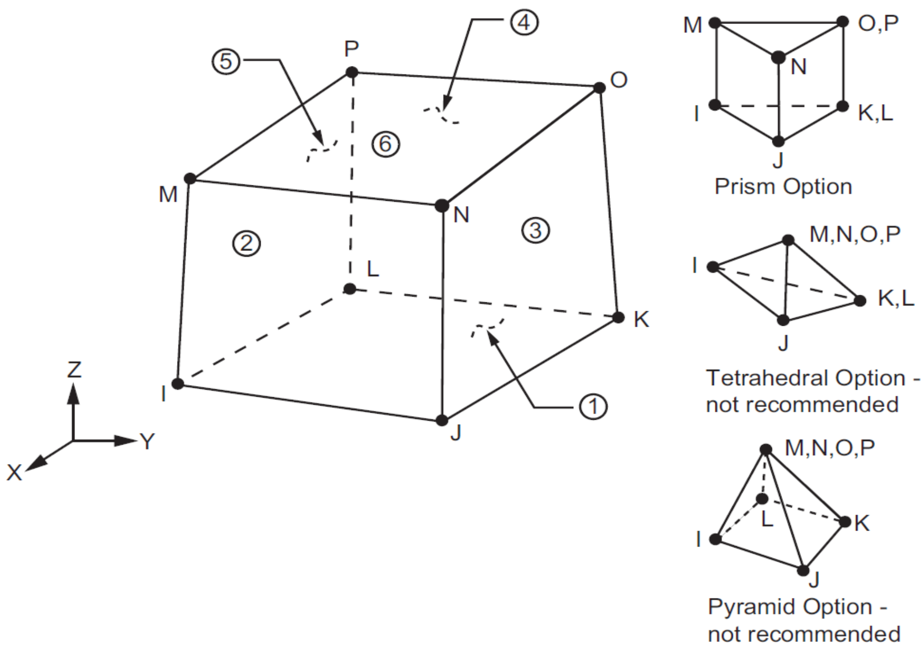

Figure 6 Solid185 element in Ansys® program.

2.3.2 Contact Surfaces

The contact surfaces between the fibers and matrices in all models are bonded. However, it is to be noted that we adopted GLUE command rather than NUMMRG command in this research. Both of these commands achieve the effect of bonding when simulating in the Ansys program. The difference between these commands is that GLUE command makes the elements sharing the same position, such as contact areas, bond to each other, while NUMMRG command actually merges the elements with same positions into a singular element. NUMMRG command occasionally produces problems. For instance, in this research, it became difficult to define which contact surface belongs to which material. For this reason, the GLUE command was chosen over NUMMRG command.

2.3.3 Meshing Elements Shapes and Sizes

Normally, the structural systems used in actual practice contain complicated geometries and displacement applied methods. The concept of finite element analysis is to break down the complicated geometries of these materials into small and simple shapes called elements. For example, in 2D geometry three and four sided elements, triangles and rectangles respectively, are considered finite elements. This can be extended to higher dimensions such as the tetrahedron and hexahedron in 3D geometry. These simple geometrical elements require far less work needed to solve problems that arise under an applied displacement defined by a handful of equations. Moreover, approximate solutions can be obtained by combining the individual results of the effects of an applied displacement on all elements as piecewise functions.

To produce highly stable and qualitative results, two methods can be considered to improve the solving processes. One, the so-called p-method, involves satisfying the boundary conditions and behaviors by making use of higher ordered equations. The other, the so-called h-method, is performed by refining the geometries into a larger number of basic elements. In general, both the p-method and h-method improve the precision of the results but require more time on their solving processes.

To determine the most appropriate element size that will save time without losing too much accuracy, different element sizes were tested to produce G_{23} values. The models that were tested needed to satisfy two conditions: firstly the models must be without voids, and secondly the model must be subjected to a shear displacement. After these conditions are satisfied, a convergence curve plot is generated with the element number defined along the x-axis and the corresponding

G_{23} values as plotted along the y-axis. In addition, the convergence curve must be satisfied by the equation below

$$G_{23} = \alpha_2 + \frac{\beta_2}{N^{\gamma_2}} \tag{111}$$

where α_2, β_2, and γ_2 are constants solved by supplementing G_{23} values of the models with finite number of elements N into Curve Fitting tool in MATLAB. Note that the command we use to control the element size and number is LESIZE command. LESIZE command is used for defining how many line segments are contained within the model as well as constructing the elements based on these line segments. In this research, each edge of the unit cell matrix was comprised of ten equal line segments whose total combined length, the length of one edge, is defined as L_m. This resulted in a percent difference which remained under 0.5%, which can be defined by the following formula the percent difference P is given by

$$P = \frac{G_{23} - \alpha_2}{G_{23}} \times 100\% \tag{112}$$

where α_2 is an indication for the expectation of the exact solution.

2.4 Boundary Conditions

2.4.1 Displacement Conditions

Considering that all elements of the models behave as ideal elastic solids, one can have confidence that their mechanical behaviors can be described by Hooke's law. To calculate the G_{23} value of all models, both load application conditions and displacements applied can be considered. Studying applied displacement conditions is a less intuitive but more powerful methodology in this research. The reasoning behind using this method is that it yields more measurably accurate results when compared to the load application method.

Therefore, homogeneous displacement boundary conditions are imposed. These equations, which are listed below, govern the displacement of the x and y edges of the model when viewed from along the z-axis (depicted in Figure 7).

$$\begin{cases} u_x = \varepsilon_{23}^0 y \\ u_y = 0 \end{cases} \text{ for all elements on } x = 0 \tag{113}$$

$$\begin{cases} u_x = 0 \\ u_y = \varepsilon_{23}^0 x \end{cases} \text{ for all elements on } y = 0 \tag{114}$$

$$\begin{cases} u_x = \varepsilon_{23}^0 y \\ u_y = \varepsilon_{23}^0 L_m \delta \end{cases} \text{ for all elements on } x = L_m \delta \tag{115}$$

$$\begin{cases} u_x = \varepsilon_{23}^0 L_m \delta \\ u_y = \varepsilon_{23}^0 x \end{cases} \text{ for all elements on } y = L_m \delta \tag{116}$$

where

$L_m =$ length of the edge of the unit cell matrix,

$\delta =$ domain size of the model,

$\varepsilon_{23}^0 =$ a dimensionless constant applied for uniform shear strain.

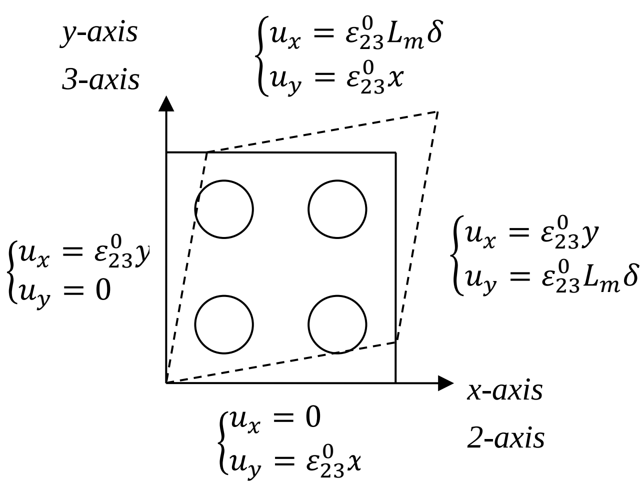

Figure 7 Strain applied on a model in Ansys® program.

2.4.2 Volumetric Weighing Average and Void Strain Rectification

To estimate the transverse shear modulus G_{23} of each model, a proper calculation method should be derived for the numerical results from the stress and strain produced by the simulation. According to Huang (2005), one concept derived from the Mori–Tanaka solution formula provided a way for the void effect on composite materials to be quantified. The formula used in calculating volumetric average stress and strain for the G_{23} calculation can be written as

$$\bar{\tau} = \frac{1}{V_t}\int_{V_t} \tau_{23,ele}\, dv_{ele} = \frac{\sum v_{ele}\tau_{23,ele}}{V_t} \tag{117}$$

$$\bar{\gamma} = \frac{1}{V_t}\int_{V_t} \gamma_{23,ele}\, dv_{ele} = \frac{\sum v_{ele}\gamma_{23,ele}}{V_t} \tag{118}$$

where

$\bar{\tau}_{23}$ = the average of shear stress applied in the x-y direction in the models,

$\bar{\gamma}_{23}$ = the average of shear strain in the x-y direction in the models,

$V_t = (L_m\delta)^3$ the total volume of the composite model,

$\tau_{23,ele}$ = the average of shear stress applied on a singular element,

$\gamma_{23,ele}$ = the average of shear strain applied on a singular element,

v_{ele} = the volume of a singular element.

Therefore the value of G_{23} can be determined by following equations

$$\tau_{23,t} = \sum v_{ele}\tau_{23,ele} \tag{119}$$

$$\gamma_{23,t} = \sum v_{ele}\gamma_{23,ele} \tag{120}$$

$$G_{23} = \frac{\bar{\tau}_{23}}{\bar{\gamma}_{23}} = \frac{\tau_{23,t}}{\gamma_{23,t}} = \frac{\sum v_{ele}\tau_{23,ele}}{\sum v_{ele}\gamma_{23,ele}} \tag{121}$$

where

$\tau_{23,t}$ = the total value of shear stress applied on the model,

$\gamma_{23,t}$ = the total value of shear strain applied on the model.

Note that the equation from the Mori–Tanaka solution can only be used to calculate the result of models without voids. For models containing voids, the equation should be modified.

The primary reason that the aforementioned equation should be modified is that although the voids have not taken the forces, they have provided various amounts of deformation. In other words, $\gamma_{23,t}$ is no longer equal to $\sum v_{ele}\gamma_{23,ele}$ for the models containing voids. It should now be rewritten as

$$\gamma_{23,t} = \sum v_{ele}\gamma_{23,ele} + \sum v_{void}\gamma_{23,void} \tag{122}$$

Therefore, the equation of shear modulus G_{23} for models containing voids should be written as

$$G_{23} = \frac{\bar{\tau}_{23}}{\bar{\gamma}_{23}} = \frac{\sum v_{ele}\tau_{23,ele}}{\sum v_{ele}\gamma_{23,ele} + \sum v_{void}\gamma_{23,void}} \tag{123}$$

However, a problem arises in that it is difficult to measure the strain caused by the deformation of the voids directly from elements $\sum v_{void}\gamma_{23,void}$. This is due to the fact that the voids have not been defined by elements because their material properties cannot be specifically defined. The solution to this difficulty is to calculate the average strain produced by elemental volume weighting $\left(\frac{\sum v_s\gamma_{23,s}}{\sum v_s}\right)$ on the matrix elements surrounding the voids. Therefore, it can be concluded that the equation to determine the G_{23} value of composite models with voids can be rewritten as follows

$$\sum v_{void}\gamma_{23,void} = \left(\frac{\sum v_s\gamma_{23,s}}{\sum v_s}\right)\sum v_{void} = \left(\frac{\sum v_s\gamma_{23,s}}{\sum v_s}\right)V_v(L_m\delta)^3 \tag{124}$$

$$G_{23} = \frac{\bar{\tau}_{23}}{\bar{\gamma}_{23}} = \frac{\tau_{23,t}}{\gamma_{23,t}} = \frac{\sum v_{ele}\tau_{ele,23}}{\sum v_{ele}\gamma_{ele,23} + \left(\frac{\sum v_s\gamma_{s,23}}{\sum v_s}\right)V_v(L_m\delta)^3} \tag{125}$$

where

$\upsilon_s =$ the volume of one element which is surrounding a void,

$\gamma_{23,s} =$ the average of shear strain applied on one of the elements which are surrounding the void.

2.5 Design of Experiments and Analysis of Variance

Design of experiments (DOE) is a mathematical statistics method that is based on numerical analysis of existing data, systematically arranging the change of independent variables, as well as observing the change of dependent variables (Montgomery, 2008). The concept of DOE method is to first examine and make a preliminary hypothesis based on existing information and then to create a series of new experiments dependent upon the conclusions of the examinations and hypothesis. Those subsequences of experiments should confirm or overthrow the hypothesis. The function of DOE is to not only minimize the costs and number of experiments, but also to achieve the desired results and conclusions.

Analysis of variance (ANOVA) is a common statistical method for models that involves dependent variables being influenced by two or more independent variables (Montgomery, 2008). Utilizing the concept of standard deviation, the ANOVA method can not only measure and differentiate the factors that have the greatest influence on the system from random noise but also determine the mixed-effect of multiple factors.

Combined with ANOVA, the DOE method utilized in this research helps us to understand the impact of void prevalence, fiber-to-matrix Young's moduli ratio, and fiber volume fraction on G_{23}. For example, these methods, when used in conjuncture, can show the importance and percent influence of the dominating factors as well as the maximum and minimum effect of void prevalence under different conditions from other variables.

Minitab® 15 Statistical Software (Minitab Inc., 2008) is statistical analysis software that provides ANOVA and DOE analysis. In this study, main effect plots and interaction plots are used for establishing the influence of each independent variable (fiber-to-matrix Young's moduli ratio E_f/E_m, fiber volume fraction V_f, and void content V_v) on the transverse shear modulus ratio $(G_{23})_\infty/G_m$. Pareto chart plots in the Minitab software are employed for defining the importance of individual factors and combinations of factors (Montgomery, 2008).

The two-level factorial design could be displayed as cube plot shown in Figure 8. The eight vertices represent the eight extreme situations for all considered conditions in this research.

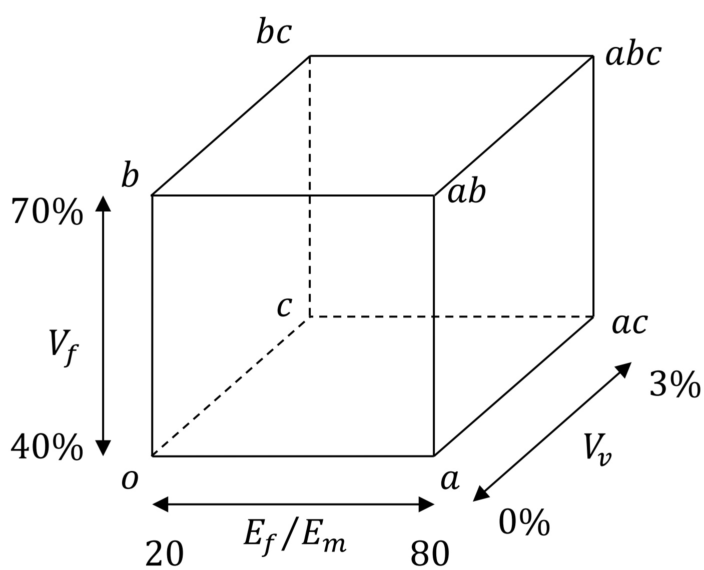

Figure 8 The cube plot for two-level three factorial design.

Based on the plot, the values on the eight extremes are

$G_{23,o}/G_m =$ the average transverse shear modulus ratio $(G_{23})_\infty/G_m$ at point o is

$$E_f/E_m = 20, V_f = 40\%, V_v = 0\%,$$

$G_{23,a}/G_m =$ the average transverse shear modulus ratio $(G_{23})_\infty/G_m$ at point a is

$$E_f/E_m = 80, V_f = 40\%, V_v = 0\%,$$

$G_{23,b}/G_m =$ the average transverse shear modulus ratio $(G_{23})_\infty/G_m$ at point b is

$E_f/E_m = 20, V_f = 70\%, V_v = 0\%,$

$G_{23,c}/G_m =$ the average transverse shear modulus ratio $(G_{23})_\infty/G_m$ at point c is

$E_f/E_m = 20, V_f = 40\%, V_v = 3\%,$

$G_{23,ab}/G_m =$ the average transverse shear modulus ratio $(G_{23})_\infty/G_m$ at point ab is

$E_f/E_m = 80, V_f = 70\%, V_v = 0\%,$

$G_{23,ac}/G_m =$ the average transverse shear modulus ratio $(G_{23})_\infty/G_m$ at point ac is

$E_f/E_m = 80, V_f = 40\%, V_v = 3\%,$

$G_{23,bc}/G_m =$ the average transverse shear modulus ratio $(G_{23})_\infty/G_m$ at point bc is

$E_f/E_m = 20, V_f = 70\%, V_v = 3\%,$

$G_{23,abc}/G_m =$ the average transverse shear modulus ratio $(G_{23})_\infty/G_m$ at point abc is

$E_f/E_m = 80, V_f = 70\%, V_v = 3\%.$

Therefore, the effects of all factors are calculated by the following equations (Montgomery, 2008):

$$A = \frac{1}{4n}\left(\frac{G_{23,a}}{G_m} + \frac{G_{23,ab}}{G_m} + \frac{G_{23,ac}}{G_m} + \frac{G_{23,abc}}{G_m} - \frac{G_{23,o}}{G_m} - \frac{G_{23,b}}{G_m} - \frac{G_{23,c}}{G_m} - \frac{G_{23,bc}}{G_m}\right) \tag{126}$$

$$B = \frac{1}{4n}\left(\frac{G_{23,b}}{G_m} + \frac{G_{23,ab}}{G_m} + \frac{G_{23,bc}}{G_m} + \frac{G_{23,abc}}{G_m} - \frac{G_{23,o}}{G_m} - \frac{G_{23,a}}{G_m} - \frac{G_{23,c}}{G_m} - \frac{G_{23,ac}}{G_m}\right) \tag{127}$$

$$C = \frac{1}{4n}\left(\frac{G_{23,c}}{G_m} + \frac{G_{23,ac}}{G_m} + \frac{G_{23,bc}}{G_m} + \frac{G_{23,abc}}{G_m} - \frac{G_{23,o}}{G_m} - \frac{G_{23,a}}{G_m} - \frac{G_{23,b}}{G_m} - \frac{G_{23,ab}}{G_m}\right) \tag{128}$$

$$AB = \frac{1}{4n}\left(\frac{G_{23,o}}{G_m} + \frac{G_{23,c}}{G_m} + \frac{G_{23,ab}}{G_m} + \frac{G_{23,abc}}{G_m} - \frac{G_{23,a}}{G_m} - \frac{G_{23,b}}{G_m} - \frac{G_{23,ac}}{G_m} - \frac{G_{23,bc}}{G_m}\right) \tag{129}$$

$$AC = \frac{1}{4n}\left(\frac{G_{23,o}}{G_m} + \frac{G_{23,b}}{G_m} + \frac{G_{23,ac}}{G_m} + \frac{G_{23,abc}}{G_m} - \frac{G_{23,a}}{G_m} - \frac{G_{23,c}}{G_m} - \frac{G_{23,ab}}{G_m} - \frac{G_{23,bc}}{G_m}\right) \tag{130}$$

$$BC = \frac{1}{4n}\left(\frac{G_{23,o}}{G_m} + \frac{G_{23,a}}{G_m} + \frac{G_{23,bc}}{G_m} + \frac{G_{23,abc}}{G_m} - \frac{G_{23,b}}{G_m} - \frac{G_{23,c}}{G_m} - \frac{G_{23,ab}}{G_m} - \frac{G_{23,ac}}{G_m}\right) \tag{131}$$

$$ABC = \frac{1}{4n}\left(\frac{G_{23,a}}{G_m} + \frac{G_{23,b}}{G_m} + \frac{G_{23,c}}{G_m} + \frac{G_{23,abc}}{G_m} - \frac{G_{23,o}}{G_m} - \frac{G_{23,ab}}{G_m} - \frac{G_{23,ac}}{G_m} - \frac{G_{23,bc}}{G_m}\right) \tag{132}$$

where A, B, and C are variables depending on specified factors only. To clarify, A is dependent only upon the fiber-to-matrix Young's moduli ratio E_f/E_m, B is only affected by the fiber volume fraction V_f, and C is influenced solely by the void content, V_v. The variables AB, AC, and BC are governed by their individual factors. ABC is the variable which is affected by all three factors.

To specifically describe the importance of all factors, comparing percentage contribution of these factors simplifies the analysis. According to Montgomery (2008), the percentage contributions of these factors are able to be simply calculated by their sum of square SS. The sum of square SS of each factors are simply the square of their effect values. For instance, the sum of square of A factor could be written as

$$SS_A = A^2 \tag{133}$$

Note that the effect values are derived from the average G_{23} value of all extreme conditions. Also, we can define the total sum of square SS_T for percentage contribution calculation

$$SS_T = SS_A + SS_B + SS_C + SS_{AB} + SS_{AC} + SS_{BC} + SS_{ABC} \tag{134}$$

Therefore, each of the percentage contribution P could be written as each of their sum of square SS divided by the total sum of square SS_T. For instance, the percentage contribution of A factor P_A could be written as

$$P_A = \frac{SS_A}{SS_T} \tag{135}$$

There are two common ways to define the importance of factors through two-level factorial design: default-generators method and specified-generators method. However, the assumption of the analysis is that the dependent variable, dimensionless shear modulus ratio G_{23}/G_m in this study, has linear relationship between the maximum and minimum of independent variables, which are fiber-to-matrix Young's moduli ratio E_f/E_m, fiber volume fraction V_f, and void content V_v.

The specify-generators method, on the other hand, allows user inputting adequate experimental data and processes, however would not produce Pareto Chart of the Effects. The reason is that the degree of freedom for the error term is larger than zero. Therefore, Minitab would produce Pareto Chart plot of the Standardized Effects.

Note that the x-axis of the Pareto Chart plot of the Standardized Effects is called student t-value in statistics. The t-value in Minitab is defined as

$$t = \frac{Coef}{SE\ Coef} \tag{136}$$

where

$Coef =$ the coefficient of each terms of regression equation, where the equation is:

$$\frac{G_{23}}{G_m} = \text{constant} + C_A\left(\frac{E_f}{E_m}\right) + C_B\left(V_f\right) + C_C(V_v)$$
$$+C_{AB}\left(\frac{E_f}{E_m}V_f\right) + C_{AC}\left(\frac{E_f}{E_m}V_v\right) + C_{BC}\left(V_f V_v\right) + C_{ABC}\left(\frac{E_f}{E_m}V_f V_v\right) \tag{137}$$

$SE\ Coef =$ the standard error of each regression coefficient terms.

Same as the processes in the default-generators method, after we have the standardized effect of each factors, specify-generators method in two-level factorial design calculate the percentage contribution P from their sum of square SS.

Moreover, the two-level factorial design would help us further explore on the decreasing of normalized transverse shear modulus NG_{23} responded from the increase of void content. In this research, two analysis methods in two-level factorial designs (default-generators and specified-generators) are adopted for this requirement but for inputting normalized transverse shear modulus NG_{23} instead of G_{23}/G_m values. The normalized transverse shear modulus NG_{23} is given by

$$NG_{23} = \frac{G_{23/m,void}}{G_{23/m,0\%}} \tag{138}$$

where

$G_{23/m,0\%} = (G_{23})_\infty / G_m$ value of composite models with no voids,

$G_{23/m,void} = (G_{23})_\infty / G_m$ value of composite models with void,

$(G_{23})_\infty / G_m =$ the estimated transverse shear modulus ratio.

Based on the definition, the effect formulas of these factors are written as

$$A = \frac{1}{4n}\left[\frac{G_{23,ac}}{G_{23,a}} + \frac{G_{23,abc}}{G_{23,ab}} - \frac{G_{23,c}}{G_{23,o}} - \frac{G_{23,bc}}{G_{23,b}}\right] \tag{139}$$

$$B = \frac{1}{4n}\left[\frac{G_{23,bc}}{G_{23,b}} + \frac{G_{23,abc}}{G_{23,ab}} - \frac{G_{23,c}}{G_{23,o}} - \frac{G_{23,ac}}{G_{23,a}}\right] \tag{140}$$

$$C = \frac{1}{4n}\left[\frac{G_{23,c}}{G_{23,o}} + \frac{G_{23,ac}}{G_{23,a}} + \frac{G_{23,bc}}{G_{23,b}} + \frac{G_{23,abc}}{G_{23,ab}}\right] \tag{141}$$

$$AB = \frac{1}{4n}\left[\frac{G_{23,c}}{G_{23,o}} + \frac{G_{23,abc}}{G_{23,ab}} - \frac{G_{23,ac}}{G_{23,a}} - \frac{G_{23,bc}}{G_{23,b}}\right] \tag{142}$$

$$AC = \frac{1}{4n}\left[\frac{G_{23,ac}}{G_{23,a}} + \frac{G_{23,abc}}{G_{23,ab}} - \frac{G_{23,c}}{G_{23,o}} - \frac{G_{23,bc}}{G_{23,b}}\right] \tag{143}$$

$$BC = \frac{1}{4n}\left[\frac{G_{23,bc}}{G_{23,b}} + \frac{G_{23,abc}}{G_{23,ab}} - \frac{G_{23,c}}{G_{23,o}} - \frac{G_{23,ac}}{G_{23,a}}\right] \tag{144}$$

$$ABC = \frac{1}{4n}\left[\frac{G_{23,c}}{G_{23,o}} + \frac{G_{23,abc}}{G_{23,ab}} - \frac{G_{23,ac}}{G_{23,a}} - \frac{G_{23,bc}}{G_{23,b}} + 2\right] \tag{145}$$

The results in this study from implementations will be discussed later in Chapter 3 (Montgomery, 2008).

CHAPTER 3 RESULTS AND DISCUSSIONS

In this research, we consider the effect of voids on the transverse shear modulus of a unidirectional composite. Before analyzing the effect of the voids, we present the model for transverse shear modulus without voids as a baseline and for comparing it with currently available analytical and empirical models. The effect on the transverse shear modulus ratio is studied as a function of the fiber-to-matrix Young's moduli, fiber volume fraction and void fraction.

To ensure pragmatic research results, this research uses the combination of three different fiber-to-matrix Young's moduli ratio ($E_f/E_m = 20, 50, 80$), three different fiber volume fractions ($V_f = 40\%, 55\%, 70\%$), and four different void contents (V_v =0%, 1%, 2%, 3%). The Young's moduli ratios encompasses polymer matrix composites ranging from glass/epoxy to graphite/epoxy. The fiber volume fractions are typical ones used in the industry. Acceptable void fractions can range from 1% to 6%, but we concentrate on 1% to 3% range that is typically acceptable for high performance structures such as those used in aerospace.

3.1 Transverse Shear Modulus Ratio of Models without Voids

In this section, we discuss the dimensionless shear modulus ratio G_{23}/G_m without the voids. Since we are limited by domain size and computational time increases as the size is increased, we use extrapolation techniques to get a limiting value of the transverse shear modulus ratio.

Fitting dimensionless shear modulus ratio G_{23}/G_m results of simplified simulation models without voids (domain size *D* 1 cell, 4 cells, 9 cells, and 16 cells) on the following equation

$$\frac{G_{23}}{G_m} = \alpha + \frac{\beta}{(D)^{\gamma}} \tag{79}$$

where α, β, and γ are constants, we predicted that the G_{23}/G_m values of the macroscopic composite materials in practical situations which contain a large number of cells. In the case of macroscopic composite materials, the cell size D of void-free models will increase in size until it reaches infinity and the curve will converge to the α value, as indicated by $(G_{23})_{\infty}/G_m$, called transverse shear modulus ratio. The subsequent numerical analysis results are shown in Table 5 and are plotted in Figure 9.

Table 5 Dimensionless shear modulus ratio G_{23}/G_m for different cell sizes in finite element simulation ($\nu_f = 0.2, \nu_m = 0.3$)

E_f/E_m	$V_f(\%)$	Cell Size D				Estimated
		1×1	2×2	3×3	4×4	$(G_{23})_{\infty}/G_m$
20	40	1.9953	1.8405	1.8078	1.7941	1.7748
	55	2.6453	2.4864	2.4433	2.4255	2.3873
	70	3.5754	3.8798	3.9740	4.0176	4.1314
50	40	2.0522	1.8839	1.8487	1.8341	1.8138
	55	2.7652	2.5953	2.5484	2.5292	2.4869
	70	3.8314	4.2720	4.4148	4.4804	4.6670
80	40	2.0670	1.8950	1.8592	1.8444	1.8236
	55	2.7970	2.6244	2.5766	2.5570	2.5132
	70	3.9016	4.3870	4.5469	4.6204	4.8386

The results shown in Table 5 indicate a decreasing tendency in the transverse shear modulus ratio as the cell sizes increases in the models where $V_f = 40\%$ and 55%; yet, there is an increasing tendency in the transverse shear modulus ratio with increasing cell sizes for the models with $V_f = 70\%$.

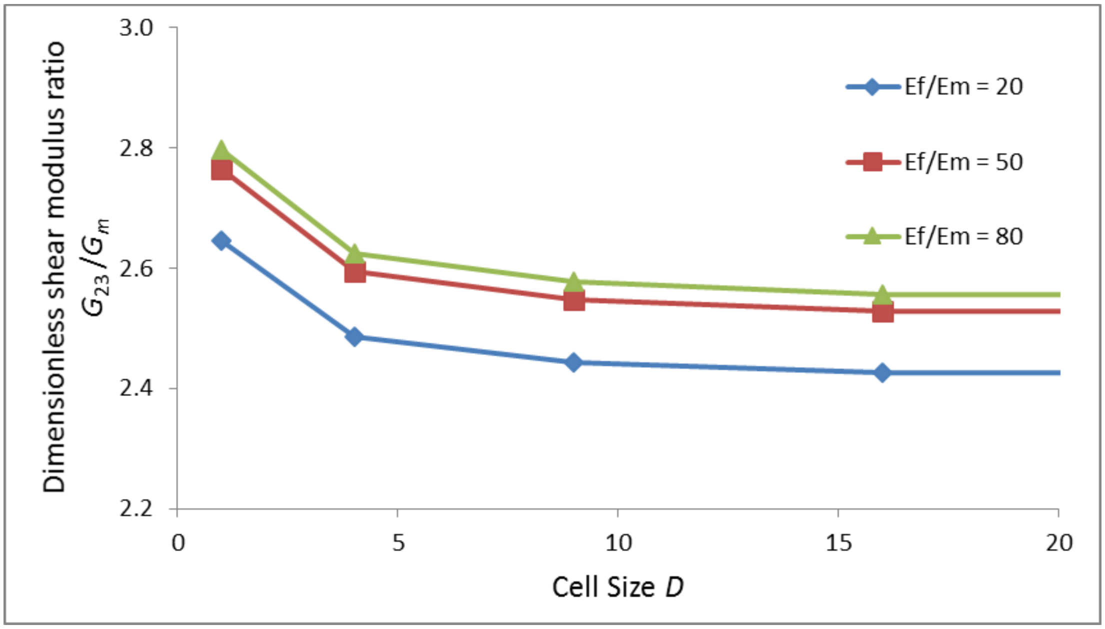

Figure 9 Dimensionless shear modulus ratio G_{23}/G_m with cell size D for $V_f = 55\%$.

The estimated transverse shear modulus ratio $(G_{23})_\infty/G_m$ of macroscopic composite materials relating to fiber-to-matrix Young's moduli ratio E_f/E_m and to fiber volume fraction V_f are reproduced in Figures 10 and 11 respectively. Both fiber-to-matrix Young's moduli ratio E_f/E_m and fiber volume fraction V_f have a positive correlation that contributes to the increase of $(G_{23})_\infty/G_m$ ratio value. Furthermore, it is obvious that the fiber volume fraction V_f factor has a more significant effect on the estimated transverse shear modulus ratio $(G_{23})_\infty/G_m$, when compared to the fiber-to-matrix Young's moduli ratio factor E_f/E_m. Also, the high value of the E_f/E_m ratio amplifies the effect of V_f factor on the value of G_{23}/G_m ratio.

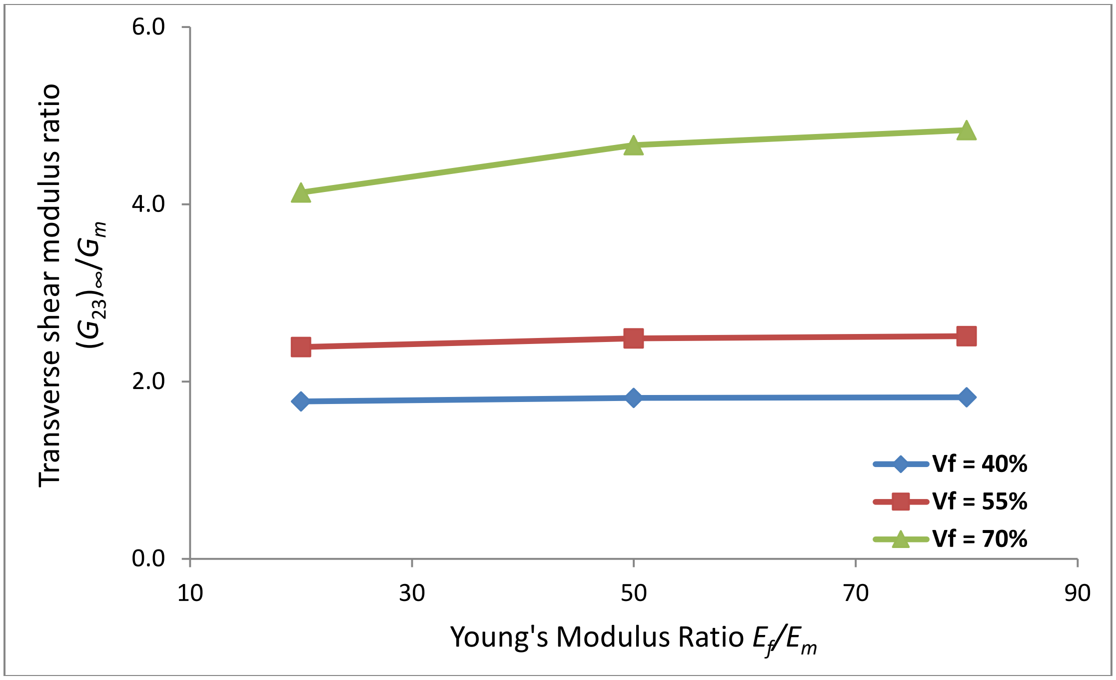

Figure 10 Estimated transverse shear modulus ratio $(G_{23})_\infty/G_m$ of macroscopic composite materials for fiber-to-matrix Young's moduli ratio E_f/E_m.

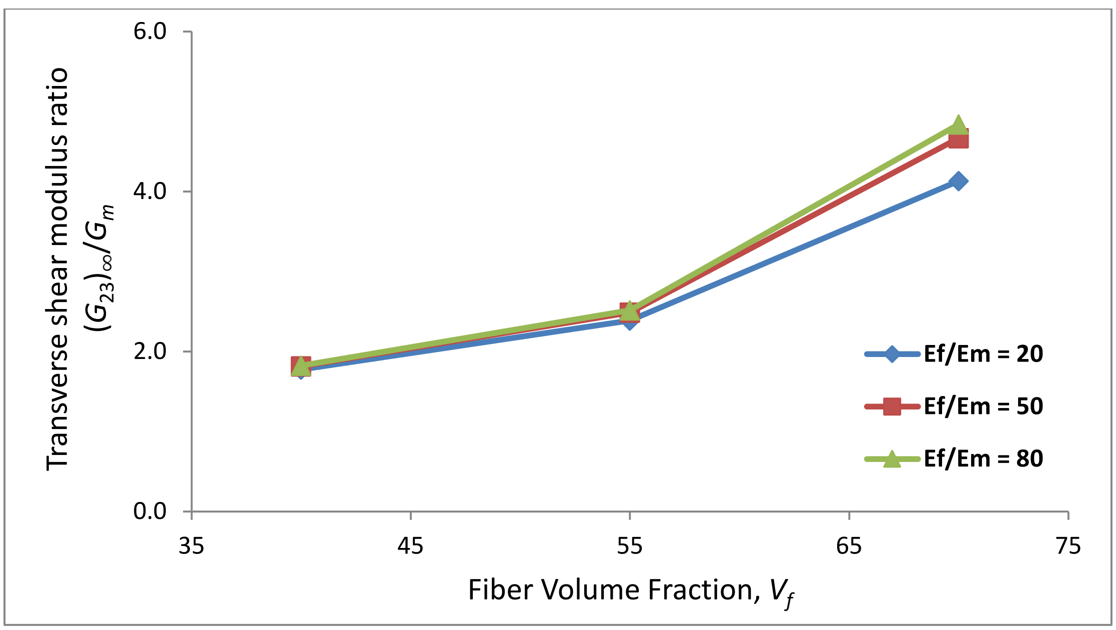

Figure 11 Estimated transverse shear modulus ratio $(G_{23})_\infty/G_m$ of macroscopic composite materials for fiber volume fraction V_f.

The theories for the composite models without voids discussed in Section 1.2 produced their own results for dimensionless shear modulus ratio G_{23}/G_m prediction. Based on the various theories, the results of G_{23}/G_m calculation for the combinations of three different fiber-to-matrix

Young's moduli ratio ($E_f/E_m = 20, 50, 80$), and three different fiber volume fractions ($V_f = 40\%, 55\%, 70\%$) are shown in Table 6. Moreover, the percentage difference between each G_{23}/G_m theoretical value and the estimated $(G_{23})_\infty/G_m$ values are given in parentheses in Table 6, where the equation is given by

$$\%\text{difference}(\%) = \frac{\left[\frac{(G_{23})_\infty}{G_m}\right] - \left(\frac{G_{23,theo}}{G_m}\right)}{\left[\frac{(G_{23})_\infty}{G_m}\right]} \times 100 \tag{146}$$

where

$G_{23,theo}$ = theoretical G_{23} value based on the theory.

Table 6 Estimated transverse shear modulus ratio from different theories ($\nu_f = 0.2, \nu_m = 0.3$) and the percentage difference (given in parenthesis) with estimated $(G_{23})_\infty/G_m$

E_f/E_m	V_f (%)	Different Theories						
		Current Model	Halpin - Tsai	Elasticity Approach	Saravanos - Chamis	Mori - Tanaka's	Bridging	Whitney and Riley
20	40	1.7748	1.9032 (-7.23%)	1.9994 (-12.65%)	2.8626 (-61.29%)	2.3686 (-33.46%)	2.9068 (-63.78%)	0.5746 (67.62%)
	55	2.3873	2.5974 (-8.80%)	2.8418 (-19.04%)	2.2620 (5.25%)	2.3686 (0.78%)	2.9068 (-21.76%)	1.0062 (57.85%)
	70	4.1314	3.8480 (6.86%)	4.3446 (-5.16%)	1.7680 (57.21%)	2.3686 (42.67%)	2.9068 (29.64%)	1.7654 (57.27%)
50	40	1.8138	1.9682 (-8.51%)	2.0852 (-14.96%)	2.9900 (-64.85%)	2.4778 (-36.61%)	3.1564 (-74.02%)	0.6266 (65.45%)
	55	2.4869	2.7456 (-10.40%)	3.0628 (-23.16%)	2.3218 (6.64%)	2.4778 (0.37%)	3.1564 (-26.92%)	1.1284 (54.63%)
	70	4.6670	4.2380 (9.19%)	4.9634 (-6.35%)	1.7966 (61.50%)	2.4778 (46.91%)	3.1564 (32.37%)	2.0722 (55.60%)
80	40	1.8236	1.9838 (-8.78%)	2.1086 (-15.63%)	3.0238 (-65.81%)	2.5064 (-37.44%)	3.2266 (-76.94%)	0.6422 (64.78%)
	55	2.5132	2.7872 (-10.90%)	3.1252 (-24.35%)	2.3374 (7.00%)	2.5064 (0.27%)	3.2266 (-28.39%)	1.1622 (53.76%)
	70	4.8386	4.3498 (10.10%)	5.1506 (-6.45%)	1.8044 (62.71%)	2.5064 (48.20%)	3.2266 (33.32%)	2.1658 (55.24%)

The results and the percentage differences shown in Table 6 indicate that the Halpin – Tsai model has high credibility for lower fiber volume fraction $(V_f = 40)$ cases, though it considerably underestimates the value for higher fiber volume fraction $(V_f = 70\%)$ cases; the Mori-Tanaka's model is most accurate for mid-range fiber volume fraction $(V_f = 55\%)$, but has a large difference in other cases; the Elasticity Approach model is able to more accurately estimate G_{23}/G_m value for higher fiber volume fraction $(V_f = 70\%)$ cases, but not for other cases.

3.2 Effect of Voids on Transverse Shear Modulus Ratio

Huang and Talreja (2005) mentioned that "For instance, for every 1% increase of void volume fraction, the reported inter-laminar shear strength reduction of 5–15% was reported in different works." In this research, we find out that the tendency of G_{23}/G_m values, as expected, decreases with the increase in void content.

As mentioned in Section 1.4, voids distribution is not going to be considered in this research, because the voids positions are not controllable during manufacturing processes. To minimize the deviation of voids distribution, we take the average from the G_{23}/G_m results of a model with three random distribution of voids under same fiber-to-matrix Young's moduli ratio E_f/E_m, fiber volume fractions V_f and void contents V_v.

After the same curve fitting process as given by Equation (79), the subsequent estimated $(G_{23})_\infty/G_m$ values with different void contents $(V_v = 0\%, 1\%, 2\%, 3\%)$ are calculated and shown in Tables 7- 9 for three void fractions of 1%, 2% and 3%, respectively.

Table 7 Dimensionless shear modulus ratio G_{23}/G_m for different cell sizes for 1% void content in finite element simulation ($\nu_f = 0.2, \nu_m = 0.3$)

E_f/E_m	V_f(%)	Cell Size				Estimated
		1×1	2×2	3×3	4×4	$(G_{23})_\infty/G_m$
20	40	1.9530	1.8207	1.7873	1.7735	1.7469
	55	2.5355	2.4120	2.3787	2.3628	2.3301
	70	3.4450	3.6909	3.7916	3.8202	3.9624
50	40	1.9995	1.8632	1.8255	1.8138	1.7841
	55	2.6548	2.5097	2.4793	2.4595	2.4352
	70	3.6818	4.0579	4.1965	4.2308	4.3836
80	40	2.0216	1.8760	1.8381	1.8210	1.7875
	55	2.6749	2.5496	2.5056	2.4918	2.4414
	70	3.7376	4.1594	4.2693	4.3973	4.7216

Table 8 Dimensionless shear modulus ratio G_{23}/G_m for different cell sizes for 2% void content in finite element simulation ($\nu_f = 0.2, \nu_m = 0.3$)

E_f/E_m	V_f(%)	Cell Size				Estimated
		1×1	2×2	3×3	4×4	$(G_{23})_\infty/G_m$
20	40	1.9123	1.7950	1.7621	1.7427	1.7009
	55	2.4930	2.3701	2.3270	2.3118	2.2586
	70	3.3456	3.6289	3.7076	3.7308	3.7908
50	40	1.9674	1.8337	1.8038	1.7821	1.7516
	55	2.5897	2.4634	2.4216	2.4163	2.3847
	70	3.5704	3.9688	4.0517	4.1076	4.1756
80	40	1.9759	1.8466	1.8111	1.7937	1.7573
	55	2.6177	2.4821	2.4427	2.4434	2.4227
	70	3.6330	4.0793	4.1649	4.2102	4.2588

Table 9 Dimensionless shear modulus ratio G_{23}/G_m for different cell sizes for 3% void content in finite element simulation ($\nu_f = 0.2, \nu_m = 0.3$)

E_f/E_m	V_f(%)	Cell Size				Estimated
		1×1	2×2	3×3	4×4	$(G_{23})_\infty/G_m$
20	40	1.8849	1.7698	1.7411	1.7157	1.6692
	55	2.4254	2.3337	2.2923	2.2648	2.0501
	70	3.2475	3.5941	3.6363	3.6620	3.6738
50	40	1.9248	1.8117	1.7766	1.7514	1.6814
	55	2.5244	2.4226	2.3814	2.3500	2.1528

Table 9 (Continued)

50	70	3.4607	3.9090	3.9712	4.0367	4.0716
80	40	1.9370	1.8213	1.7839	1.7646	1.7100
	55	2.5490	2.4419	2.4050	2.3682	2.1791
	70	3.5283	3.9885	4.0882	4.0841	4.1236

Similar to the results shown in Table 5, the dimensionless shear modulus ratio G_{23}/G_m decreases as cell size is increased in the models where $V_f = 40\%$ and 55%, and yet show an opposite tendency in the models where $V_f = 70\%$.

After reorganizing the estimated transverse shear modulus ratio $(G_{23})_\infty/G_m$ from Tables 5-9, the relationship of various void contents and their effect on undermining the values of transverse shear modulus listed in Table 10 would be conducive to this observation. The percentage difference shown in Table 10 for $(G_{23})_\infty/G_m$ value is given by

$$\%diff = \frac{G_{23/m,0\%} - G_{23/m,void}}{G_{23/m,0\%}} \times 100\% \tag{147}$$

where

$G_{23/m,0\%}$ = the $(G_{23})_\infty/G_m$ value of composite models with no voids,

$G_{23/m,void}$ = the $(G_{23})_\infty/G_m$ value of composite models with following void contents.

Table 10 Estimated transverse shear modulus ratio $(G_{23})_\infty/G_m$ in finite element simulation for different void contents and their percentage difference with void-free models

E_f/E_m	$V_f(\%)$	Void content V_v			
		0%	1%	2%	3%
20	40	1.7748 (-)	1.7469 (1.57%)	1.7009 (4.16%)	1.6692 (5.95%)
	55	2.3873 (-)	2.3301 (2.40%)	2.2586 (5.39%)	2.0501 (14.13%)
	70	4.1314 (-)	3.9624 (4.09%)	3.7908 (8.24%)	3.6738 (11.08%)

Table 10 (Continued)

50	40	1.8138 (-)	1.7841 (1.63%)	1.7516 (3.43%)	1.6814 (7.30%)
	55	2.4869 (-)	2.4352 (2.08%)	2.3847 (4.11%)	2.1528 (13.43%)
	70	4.6670 (-)	4.3836 (6.07%)	4.1756 (10.53%)	4.0716 (12.76%)
80	40	1.8236 (-)	1.7875 (1.98%)	1.7573 (3.64%)	1.7100 (6.23%)
	55	2.5132 (-)	2.4414 (2.86%)	2.4227 (3.60%)	2.1791 (13.29%)
	70	4.8386 (-)	4.7216 (2.42%)	4.2588 (11.98%)	4.1236 (14.78%)

Some conclusions could be drawn from the Table 10. For all of the cases, void contents V_v bring negative effect on transverse shear modulus ratio $(G_{23})_\infty/G_m$ values. The 1% void content reflects 1% to 4% decreasing tendency on estimated transverse shear modulus ratio $(G_{23})_\infty/G_m$; the 2% void contents reflect 3% to 7% decreasing tendency on estimated $(G_{23})_\infty/G_m$; the 3% void contents reflect 5% to 14% decreasing tendency on $(G_{23})_\infty/G_m$. Furthermore, for most of the cases, the increasing tendency along fiber volume fractions V_f aggravates the sensitivity of the negative effect of void contents, especially when $V_f = 70\%$.

Based on the Table 10, plotting the decreasing tendency of $(G_{23})_\infty/G_m$ as void content increases are shown in Figures 12 and 13. The figures compare it for the various fiber-to-matrix Young's moduli ratio E_f/E_m (shown on Figure 12, for $V_f = 55\%$) and the various fiber volume fractions V_f (shown on Figure 13, for $E_f/E_m = 50$).

The findings indicate that the most powerful factor of the three is fiber volume fraction V_f, the second most influencing factor is the void fraction V_v, while the fiber-to-matrix Young's moduli ratio E_f/E_m has the smallest effect.

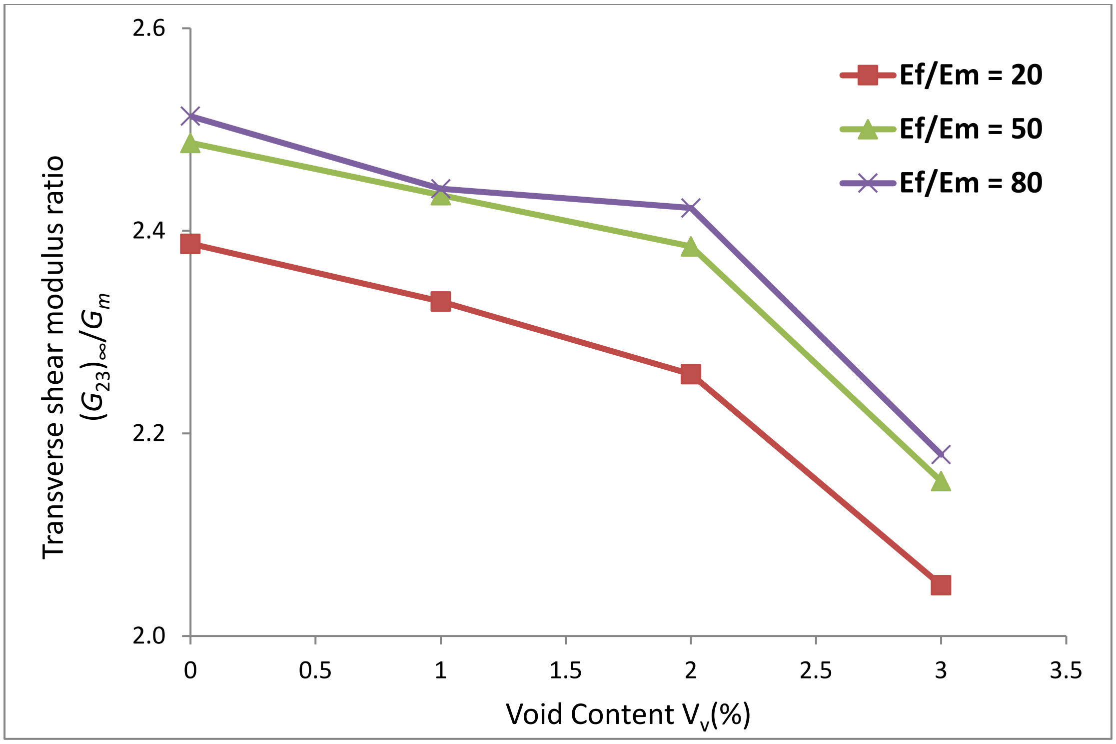

Figure 12 Estimated transverse shear modulus ratio $(G_{23})_\infty/G_m$ as a function of void contents V_v for fiber volume fraction $V_f = 55\%$.

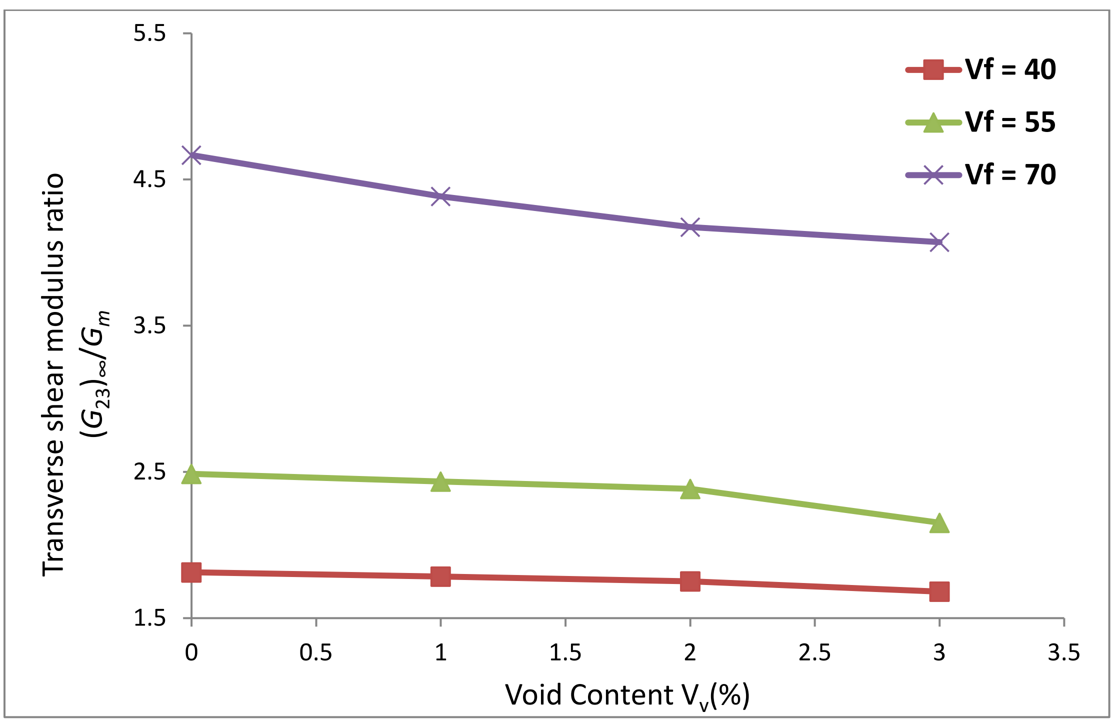

Figure 13 Estimated transverse shear modulus $(G_{23})_\infty/G_m$ as a function of void contents V_v for fiber-to-matrix Young's moduli ratio $E_f/E_m = 50$.

3.3 Design of Experiments

3.3.1 Analysis on Main Effect and Interaction Effect

The main effect plot and the interaction plot produced from Minitab describe the influence and characteristics of the three factors (fiber-to-matrix Young's moduli ratio E_f/E_m, fiber volume fractions V_f, and void contents V_v). According to the main effect plot shown in Figure 14, transverse shear modulus ratio $(G_{23})_\infty/G_m$ has higher sensitivity to the change of fiber volume fraction V_f as compared to the change of two others, which is same as the conclusion in Section 3.2. The main effect plot also indicates that the value of $(G_{23})_\infty/G_m$ increases exponentially with increasing V_f. Therefore, fiber volume fraction V_f is a key factor for design of composite materials when pursuing high transverse shear modulus ratio.

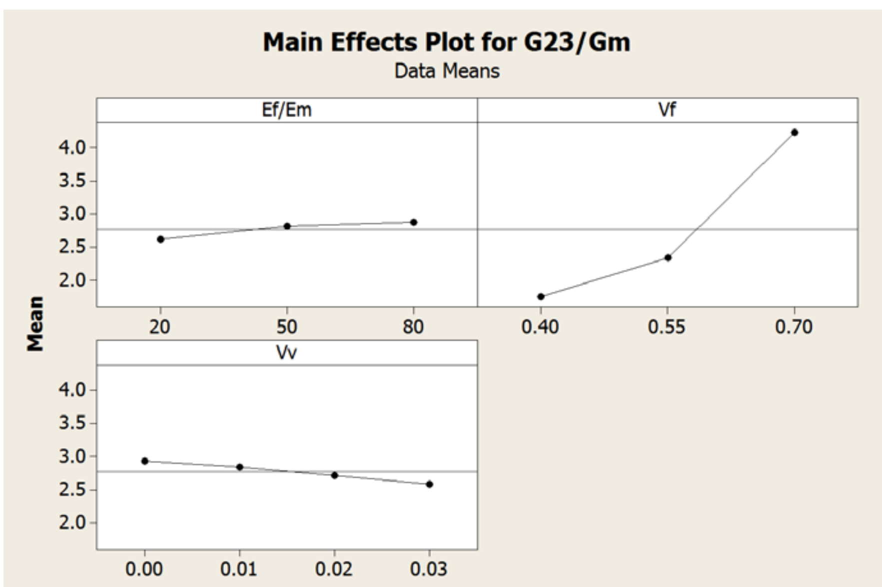

Figure 14 Main effect plots of fiber-to-matrix Young's moduli ratio E_f/E_m, fiber volume fraction V_f, and void content V_v on estimated transverse shear modulus ratio $(G_{23})_\infty/G_m$.

The results of interaction plot from the three factors are shown in Figure 15. The findings indicate that high value of fiber volume fraction V_f would increase G_{23}/G_m when fiber-to-matrix

Young's moduli ratio E_f/E_m is increasing. On the other hand, high value of E_f/E_m ratio would get higher results of G_{23}/G_m when V_f increases. However, high value of fiber volume fraction V_f would aggressively decrease the effect of $(G_{23})_\infty/G_m$ when void content V_v is increasing. The phenomenon is reasonable because comparing the model with same void content V_v, the higher value of V_f implies higher value of f_v.

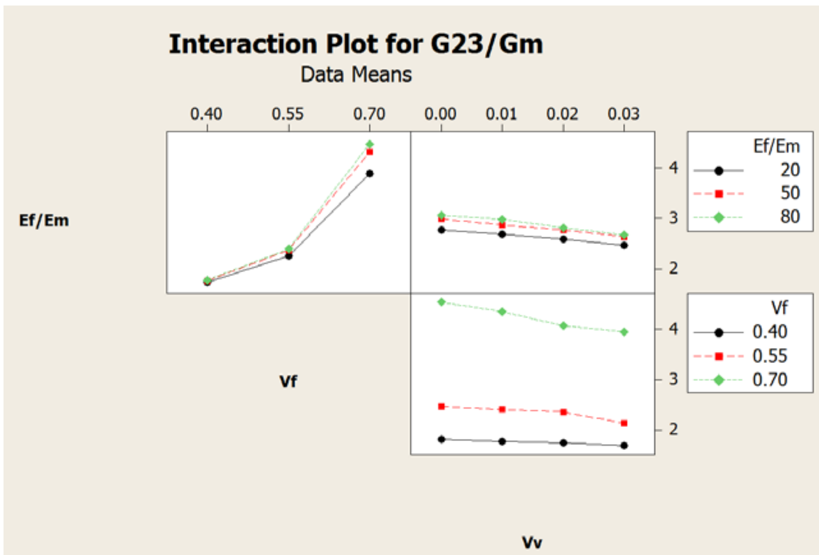

Figure 15 Interaction plots of fiber-to-matrix Young's moduli ratio E_f/E_m, fiber volume fraction V_f, and void content V_v on estimated transverse shear modulus ratio $(G_{23})_\infty/G_m$.

3.3.2 Analysis on Estimated Transverse Shear Modulus Results

Pareto Chart Plots in Minitab software is used for defining the importance of individual and combination of factors. As mentioned in Section 2.5, specify-generators method (Montgomery, 2008) is used to describe the importance through two-level factorial design, where the cube plot is shown in Figure 16. The results from the specify-generators method are of equal or higher considerable referential importance as compared to the default-generators method. The reason was mentioned in Section 2.5 that the regression equation curve instead of linear reflection as an assumption seems a more plausible way to describe the dependent variable $(G_{23})_\infty/G_m$ from these factors.

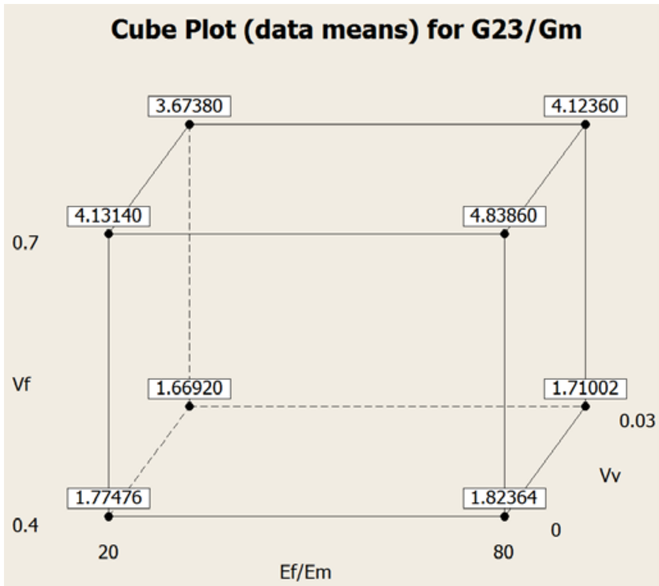

Figure 16 Cube plot of transverse shear modulus ratio $(G_{23})_\infty/G_m$ for two-level factorial design in Minitab® program.

The findings from two-level factorial design are shown in Tables 11 and 12, and Figures 17 and 18. The Pareto Chart of the Effect from specify-generators is shown on Figure 17. The percentage contribution of the factors is shown in Figure 18.

Note that to simplify the display of table, we call fiber-to-matrix Young's moduli ratio E_f/E_m as factor *A*; fiber volume fraction V_f as factor *B*; void content V_v as factor *C*.

Table 11 Estimated effects and coefficients for estimated transverse shear modulus ratio $(G_{23})_\infty/G_m$ based on two-level factorial design

Factor	Effect	Coef	Standardized Effect
constant		-1.2377	46.40
$A\ (E_f/E_m)$	0.2584	-0.0165	1.7649
$B\ (V_f)$	2.4831	7.1420	16.959

Table 11 (Continued)

$C\ (V_v)$	-0.3489	5.5082	-2.1751
$A*B$	0.2747	0.0393	1.5318
$A*C$	-0.0505	0.2663	-0.25696
$B*C$	-0.2492	-26.0607	-1.2683
$A*B*C$	-0.0791	-0.5862	-0.32890

Table 12 Estimated standardized effects and percent contribution for estimated transverse shear modulus ratio $(G_{23})_\infty/G_m$ based on two-level factorial design

Factor	Standardized Effect	Sum of Squares	Percent Contribution
$A\ (E_f/E_m)$	1.7649	3.1149	1.04%
$B\ (V_f)$	16.959	287.5975	96.00%
$C\ (V_v)$	-2.1751	4.7311	1.58%
$A*B$	1.5318	2.3464	0.78%
$A*C$	-0.25696	0.0660	0.02%
$B*C$	-1.2683	1.6086	0.54%
$A*B*C$	-0.32890	0.1082	0.04%

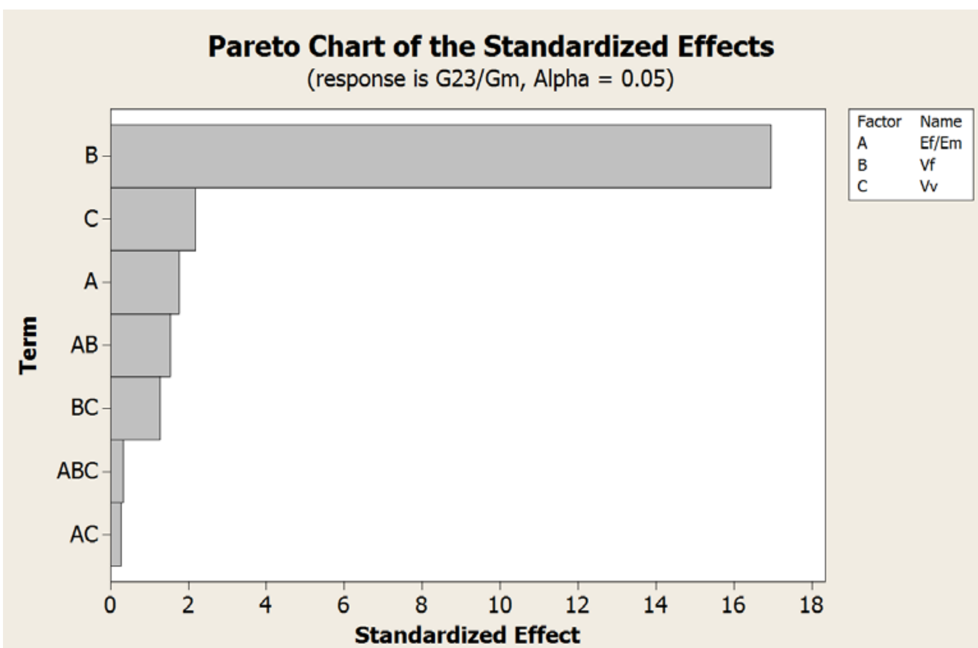

Figure 17 Pareto Chart of the Standardized Effect from two-level factorial design.

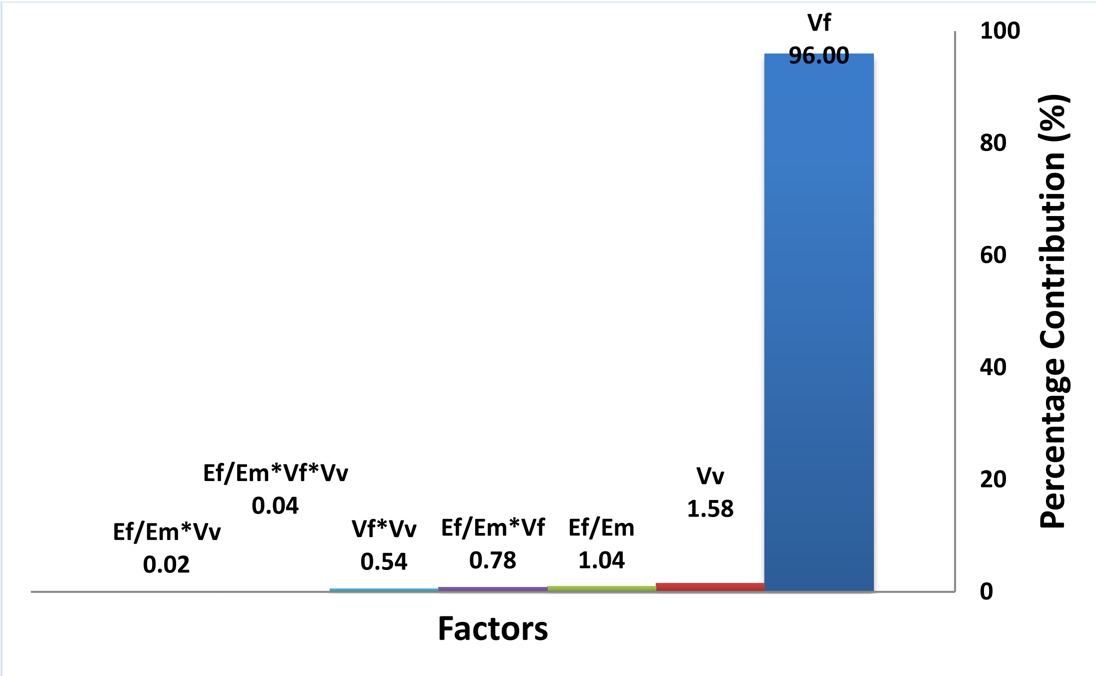

Figure 18 Percentage contribution of transverse shear modulus ratio $(G_{23})_\infty/G_m$ with their factors from two-level factorial design.

The findings indicate that fiber volume fraction V_f has the most influence on $(G_{23})_\infty/G_m$ and the percentage contribution of V_f on $(G_{23})_\infty/G_m$ is 96%. The importance of fiber-to-matrix Young's moduli ratio E_f/E_m and of void content V_v is lower than 2%.

3.3.3 Analysis on Normalized Transverse Shear Modulus Results

Table 13 tabulates the same simulation document and calculates the normalized transverse shear modulus NG_{23} value. The normalization is done by the corresponding transverse shear modulus ratio with no voids. Also, same as the processing of dealing with $(G_{23})_\infty/G_m$ previously, the cube plot shown on Figure 19 is produced to understand how the static method works in two-level factorial design.

To facilitate a better understanding of how the transverse shear modulus ratio gets affected by fiber-to-matrix Young's moduli ratio, fiber volume fraction and void volume fraction, we normalize $(G_{23})_\infty/G_m$ by the $(G_{23})_\infty/G_m$ of the composite without any voids, and hence call it

NG_{23}, which is given by

$$NG_{23} = \frac{G_{23/m,void}}{G_{23/m,0\%}} \tag{138}$$

where

$G_{23/m,0\%} = (G_{23})_\infty/G_m$ value of composite models with no voids,

$G_{23/m,void} = (G_{23})_\infty/G_m$ value of composite models with void,

$(G_{23})_\infty/G_m =$ transverse shear modulus ratio.

Table 13 shows NG_{23} as a function of fiber-to-matrix Young's moduli ratio, fiber volume fraction and void volume fraction.

Table 13 Estimated normalized transverse shear modulus NG_{23} of finite element simulation for different void contents

E_f/E_m	V_f (%)	Void content V_v			
		0%	1%	2%	3%
20	40	1	0.9843	0.9584	0.9405
	55	1	0.9760	0.9461	0.8587
	70	1	0.9591	0.9176	0.8892
50	40	1	0.9837	0.9657	0.9270
	55	1	0.9792	0.9589	0.8657
	70	1	0.9393	0.8947	0.8724
80	40	1	0.9802	0.9636	0.9377
	55	1	0.9714	0.9640	0.8671
	70	1	0.9758	0.8802	0.8522

From Figure 19, it is noticed that NG_{23} is affected more at higher fiber volume fraction while the influence of Young's moduli ratio is minimal. The estimated effects results, the Pareto chart plot of the effects of normalized NG_{23} and the percentage contribution plot from two-level factorial design are shown in Tables 14 and 15, and Figures 20 and 21.

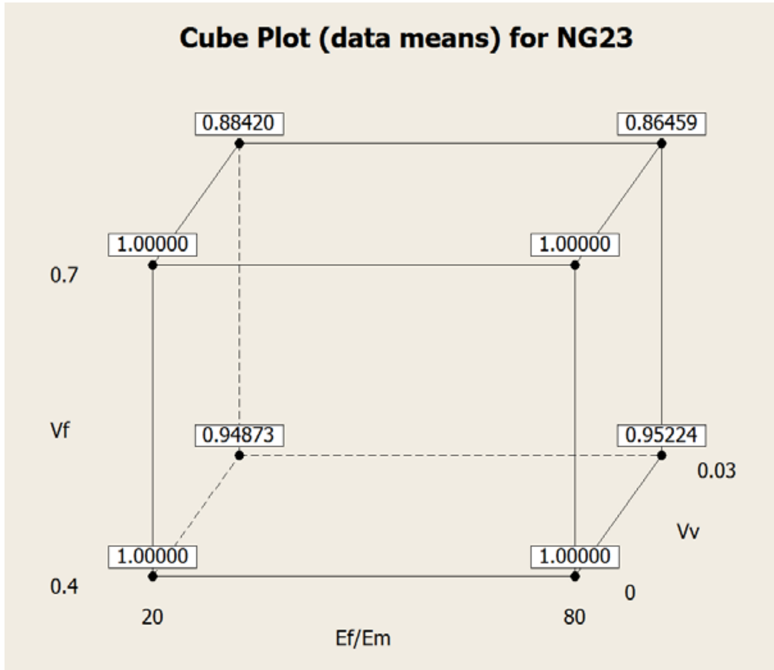

Figure 19 Cube plot of normalized transverse shear modulus NG_{23} for two-level factorial design.

Table 14 Estimated effects and coefficients for normalized transverse shear modulus NG_{23} based on two-level factorial design

Factor	Effect	Coef	Standardized Effect
constant		1.02578	341.72
$A\ (E_f/E_m)$	-0.00315	-0.00029	-0.46196
$B\ (V_f)$	-0.03839	-0.04239	-5.6361
$C\ (V_v)$	-0.10893	-1.59369	-14.599
$A*B$	-0.00699	0.00061	-0.83837
$A*C$	-0.00584	0.04425	-0.63893
$B*C$	-0.03477	-3.11462	-3.8050
$A*B*C$	-0.01245	-0.09225	-1.1127

Table 15 Estimated standardized effects and percent contribution for normalized transverse shear modulus NG_{23} based on two-level factorial design

Factor	Standardized Effect	Sum of Squares	Percent Contribution
$A\ (E_f/E_m)$	-0.46196	0.21340	0.08%
$B\ (V_f)$	-5.6361	31.76540	12.13%

Table 15 (Continued)

C (V_v)	-14.599	213.13956	81.37%
A*B	-0.83837	0.70286	0.27%
A*C	-0.63893	0.40823	0.16%
B*C	-3.8050	14.47833	5.53%
A*B*C	-1.1127	1.23815	0.47%

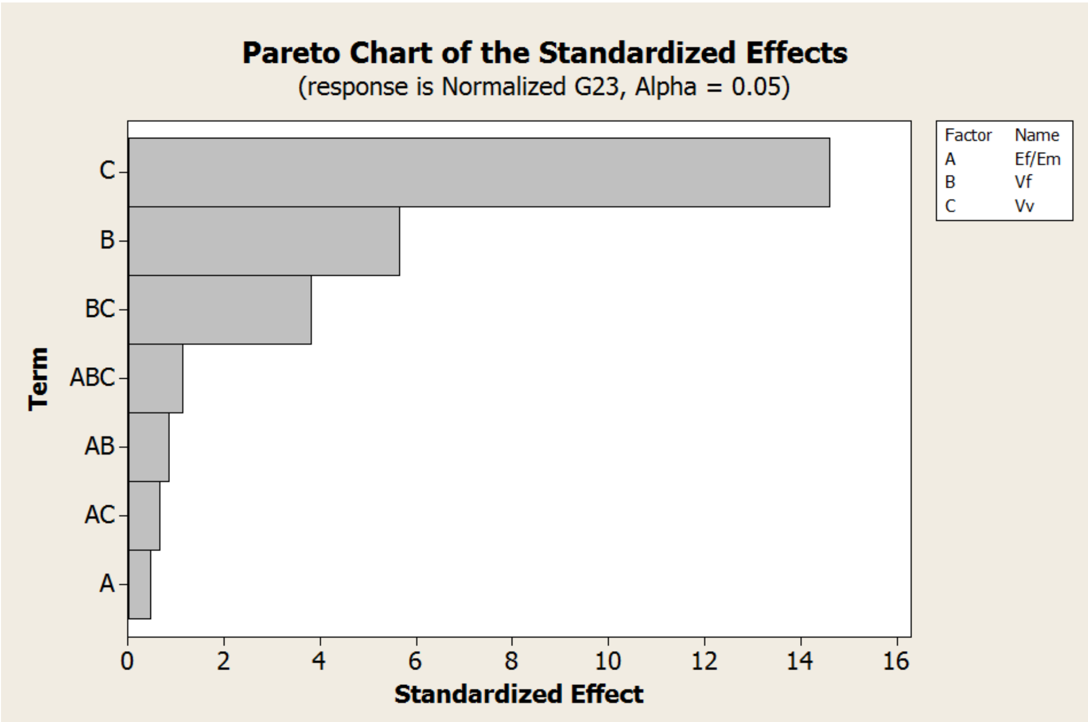

Figure 20 Pareto Chart of the Standardized Effect of normalized transverse shear modulus NG_{23} for two-level factorial design.

The findings indicate that the void content factor V_v is the significant factor of decreasing the normalized transverse shear modulus NG_{23}, making up to 81% of the percentage contribution. Based on the analysis, other factors influencing NG_{23} are fiber volume fraction V_f with 12% contribution, and combined factor V_f*V_v with 5.5% contribution. However, the influence of fiber-to-matrix Young's moduli ratio E_f/E_m is minimal.

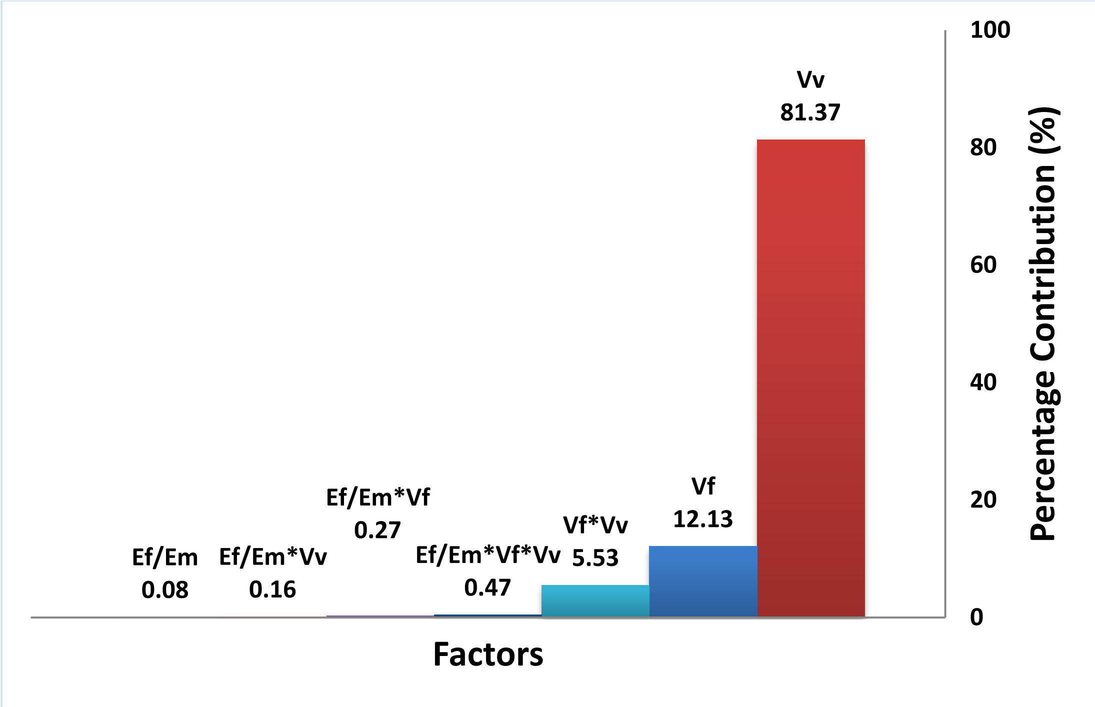

Figure 21 Percentage contribution of normalized transverse shear modulus NG_{23} with their factors for two-level factorial design.

CHAPTER 4 CONCLUSIONS AND RECOMMENDATIONS

The usefulness of mathematical models of elasticity for composite materials is dependent on the accurate estimation of elastic moduli of unidirectional composites. In this study, we concentrated on one of the five elastic moduli, namely transverse shear modulus, and quantify the effect of three parameters – fiber-to-matrix Young's moduli ratio, fiber volume fraction and void fraction. To reach the research goal, three steps were taken.

The first step was to compare the estimate of the transverse shear modulus from existing analytical and empirical models with finite element models to comprehend which theories are more accurate. The study concentrated on typical values for polymer matrix composites: fiber-to-matrix Young's moduli ratio from 20 to 80, fiber volume fraction from 40% to 70%. The second step was to evaluate the significance of void content in addition to the fiber-to-matrix moduli Young's moduli ratio and the fiber volume fraction. The third step was to conduct a design of experiments study to evaluate the influence of these three parameters and their combinations.

The conclusions of the study are as follows.

- For no void content, the estimate of the transverse shear modulus by Halpin-Tsai model was found to have high credibility for lower fiber volume fractions; the Mori-Tanaka's model was most accurate for mid-range fiber volume fractions; the Elasticity Approach model was more accurate for high fiber volume fractions.
- Using design of experiments, the fiber volume fraction is the most dominating of the three parameters on the transverse shear modulus with more than 96% contribution. It implies that the fiber-to-matrix Young's moduli ratio and void content are negligible

contributors.

- Since the transverse shear modulus is dependent so heavily on fiber volume fraction, a normalized transverse shear modulus was calculated for a design of experiments study. The normalization was done with respect to the shear modulus of a corresponding composite with no voids. The percentage contribution of the void content was now found to be more than 80%, while fiber-to-matrix Young's moduli ratio had negligible contribution.

Future work based on this study could explore more pragmatic geometry of voids. For instance, this study assumes that the voids are of uniform radii and lengths, and are of cylindrical shape. Voids could be generated randomly with differing radii and lengths, or by using experimental observation of void geometry. Another recommendation would be to choose periodic distribution of fibers which results in orthotropic behavior as opposed to that of transversely isotropic materials. These include rectangular as opposed to square or hexagonal distribution of fibers.

REFERENCES

Agboola, B. O., Jack, D. A., & Baylor University. (2011). *Investigation of dense suspension rotary diffusion models for fiber orientation predictions during injection molding of short-fiber reinforced polymeric composites*. Waco, Tex: Baylor University.

ANSYS Mechanical APDL, Release 17.0 [Computer software] (2016) Canonsburg, PA: ANSYS Inc.

Benveniste, Y. (1987). A new approach to the application of Mori-Tanaka's theory in composite materials. *Mechanics of Materials, 6*(2), 147-157.

Bhalchandra, S. A., Shiradhonkar, Y., & Daimi, S. S. (2014). Comparison of properties of transversely isotropic lamina using method of cells and composite cylinder assemblage. *International Journal of Advanced Science and Technology*, *64*(5), 43-58.

Bowles, K. J., & Frimpong, S. (1992). Void effects on the interlaminar shear strength of unidirectional graphite-fiber-reinforced composites. *Journal of Composite Materials*, *26*(10), 1487-1509.

Chandra, R., Singh, S. P., & Gupta, K. (2002). Micromechanical damping models for fiber-reinforced composites: a comparative study. *Composites Part A: Applied Science and Manufacturing*, *33*(6), 787-796.

Clarke, J. L. (1996). *Structural design of polymer composites: Eurocomp design code and background document*. London: E & FN Spon.

Christensen, R. M. (1990). A critical evaluation for a class of micro-mechanics models. *Journal of the Mechanics and Physics of Solids, 38*(3), 379-404.

Ghiorse, S. R., & Army Materials Research Agency, Watertown, MA (United States). Materials Technology Lab. (1991). *A comparison of void measurement Methods for Carbon/Epoxy Composites*. Ft. Belvoir: Defense Technical Information Center.

Hamidi, Y. K., Aktas, L., & Altan, M. C. (2004). Formation of microscopic voids in resin transfer molded composites. *Journal of Engineering Materials and Technology, 126*(4), 420-426.

Hamidi, Y. K., Aktas, L., & Altan, M. C. (2005). Three-dimensional features of void morphology in resin transfer molded composites. *Composites Science and Technology*, *65*(7), 1306-1320.

Hashin, Z., & Rosen, B. W. (1964). The elastic moduli of fiber-reinforced materials. *Journal of Applied Mechanics, 31*(2), 223-232.

Huang, H., & Talreja, R. (2005). Effects of void geometry on elastic properties of unidirectional fiber reinforced composites. *Composites Science and Technology*, *65*(13), 1964-1981.

Huang, Z. M. (2000). A unified micromechanical model for the mechanical properties of two constituent composite materials. Part I: Elastic behavior. *Journal of Thermoplastic Composite Materials*, *13*(4), 252-271.

Huang, Z. M. (2001). Simulation of the mechanical properties of fibrous composites by the bridging micromechanics model. *Composites Part A: Applied Science and Manufacturing*, *32*(2), 143-172.

Ishai, O., & Cohen, L. J. (1967). Elastic properties of filled and porous epoxy composites. *International Journal of Mechanical Sciences*, *9*(8), 539-546.

Jena, A. K., & Chaturvedi, M. C. (1992). *Phase transformation in materials*. Englewood Cliffs, N.J: Prentice Hall.

Jiang, M., Alzebdeh, K., Jasiuk, I., & Ostoja-Starzewski, M. (2001). *Scale and boundary conditions effects in elastic properties of random composites composites*. *Acta Mechanica*,*148*(1-4), 63-78.

Kardos, J. L., Duduković, M. P., & Dave, R. (1986). Void growth and resin transport during processing of thermosetting—matrix composites. In *Epoxy Resins and Composites IV* (pp. 101-123). Berlin, Heidelberg, New York: Springer.

Kaw, A. K. (2005). *Mechanics of composite materials* (2nd ed.). Boca Raton, FL: CRC Press.

Lim, L. G., & Dunne, F. P. E. (1996). Modelling void nucleation and growth processes in a particle-reinforced metal matrix composite material. *Computational Materials Science*, *5*(1), 177-186.

Liu, L., & Huang, Z. (2014). A Note on mori-tanaka's method. *Acta Mechanica Solida Sinica*, *27*(3), 234-244.

Liu, L., Zhang, B. M., Wang, D. F., & Wu, Z. J. (2006). Effects of cure cycles on void content and mechanical properties of composite laminates. *Composite Structures*, *73*(3), 303-309.

Little, J. E., Yuan, X., & Jones, M. I. (2012). Characterisation of voids in fibre reinforced composite materials. *Ndt and E International*, *46*(1), 122-127.

Lusti, H. R. (2003). *Property predictions for short fiber and platelet filled materials by finite element calculations* (Doctoral dissertation, Diss., Technische Wissenschaften ETH Zürich, Nr. 15078, 2003).

MATLAB, Release 2014a [Computer software] (2014) Natick, MA: The MathWorks, Inc.

Meola, C., & Toscano, C. (2014). Flash thermography to evaluate porosity in carbon fiber reinforced polymer (CFRPs). *Materials, 7*(3), 1483-1501.

MINITAB statistical software, Release 15 [Computer software] (2008) State College, PA: Minitab Inc.

Montgomery, D. C. (2008). *Design and analysis of experiments*. Hoboken, NJ: Wiley.

Narra, G. (2012). *Stress bridging in particulate composites and calculation of G_{23} in particulate composites.* (Doctoral dissertation, The University of Utah).

Pettermann, H. E., Huber, C. O., Luxner, M. H., Nogales, S., & Böhm, H. J. (2010). An incremental mori-tanaka homogenization scheme for finite: strain thermoelastoplasticity of mmcs. *Materials*, *3*(1), 434-451.

Porter, D. A., Easterling, K. E., & Sherif, M. (2009). *Phase transformations in metals and alloys*. New York: Van Nostrand Reinhold.

Purslow, D. (1984). On the optical assessment of the void content in composite materials. *Composites*, *15*(3), 207-210.

Purslow, D. (1977). *The shear properties of unidirectional carbon fibre reinforced plastics and their experimental determination*. London: Her Majesty's Stationery Office.

Rafic, Y., Ali, H., Fadi, H. C., & Farouk, F. (2012). *Comparative review study on elastic properties modeling for unidirectional composite materials*. INTECH Open Access Publisher.

Seiler, F., Werner, U., Patz, G., Riley, M. B., & Whitney, J. M. (1966). Elastic properties of fiber reinforced composite materials. *Aiaa Journal*, *4*(9), 1537-1542.

Selvadurai, A. P. S., & Nikopour, H. (2012). Transverse elasticity of a unidirectionally reinforced composite with an irregular fibre arrangement: experiments, theory and computations. *Composite Structures*, *94*(6), 1973-1981

Sendeckyj, G. P., Wang, S. S., Steven, J. W., Stinchcomb, W. W., Pagano, N. J., Saravanos, D. A., & Chamis, C. C. (1990). Unified micromechanics of damping for unidirectional and off-axis fiber composites. *Journal of Composites Technology and Research*, *12*(1), 31.

Shakya, N., Roux, J. A., & Jeswani, A. L. (2013). Effect of resin viscosity in fiber reinforcement compaction in resin injection pultrusion process. *Applied Composite Materials, 20*(6), 1173-1193.

Zhou, Y.-X., & Huang, Z.-M. (2012). A bridging model prediction of the ultimate strength of composite laminates subjected to triaxial loads. *Journal of Composite Materials, 46*(19-20), 2343-2378.

Zitko, J. & Kaw, A. K. (2012). *Effects of Random Cross-Sectioned Distributions, Fiber Misalignment and Interphases in Three-Dimensional Composite Models on Transverse Shear Modulus.* (Master dissertation, University of South Florida).

APPENDIX A: COPYRIGHT PERMISSIONS

A.1 Permission from Ansys, Inc.

Figure 5 is screenshot created with the software Ansys APDL 17.0, and Figure 6 is a copied figure from figure 185.1 on p.984 in ANSYS Mechanical APDL Element Reference 15.0.

USF

Jui-He Tai <juihetai@mail.usf.edu>

Request for copyright permission to image and screenshots from Ansys APDL and their element reference

Paul Lethbridge <paul.lethbridge@ansys.com> Fri, Jun 17, 2016 at 3:55 PM
To: Jui-He Tai <juihetai@mail.usf.edu>

Dear Jui-he Tai,

Thanks VERY much for contacting us, and for using ANSYS simulation products for your research.

You may reuse such ANSYS product images, screen shots, and short excerpts from our documentation under "fair use" terms, as long as you include a statement such as "*ANSYS product and training documentation are used courtesy of ANSYS, Inc.* "

Our general citation guidelines are here: http://www.ansys.com/Products/Academic/Citations

So please use the fair use statement above in your thesis, and this email from me as your permission to proceed.
I and my colleagues here at ANSYS wish you all the best in completing your thesis and a successful outcome.

Kind regards,

Paul.

Dr. Paul Lethbridge
Senior Manager - Academic and Startup Programs
ANSYS, Inc.

Mobile phone: 503 708 4988

---

www.ansys.com
The information transmitted is intended only for the person or entity to which it is addressed and may contain confidential and/or privileged material. Any review, retransmission, dissemination or other use of, or taking of any action in reliance upon, this information by persons or entities other than the intended recipient is prohibited. If you received this in error, please contact the sender and delete the material from any computer.

A.2 Permission from Composites Science and Technology

Figure 4 is figure 4 in the article, "Effect of void geometry on elastic properties of unidirectional fiber reinforced composites" by Hansong Huang, and Ramesh Talreja, which is published by Composites Science and Technology journal.

6/18/2016 RightsLink - Your Account

ELSEVIER LICENSE
TERMS AND CONDITIONS

Jun 18, 2016

This Agreement between Jui ("You") and Elsevier ("Elsevier") consists of your license details and the terms and conditions provided by Elsevier and Copyright Clearance Center.

License Number	3887230823405
License date	Jun 13, 2016
Licensed Content Publisher	Elsevier
Licensed Content Publication	Composites Science and Technology
Licensed Content Title	Effects of void geometry on elastic properties of unidirectional fiber reinforced composites
Licensed Content Author	Hansong Huang,Ramesh Talreja
Licensed Content Date	October 2005
Licensed Content Volume Number	65
Licensed Content Issue Number	13
Licensed Content Pages	18
Start Page	1964
End Page	1981
Type of Use	reuse in a thesis/dissertation
Portion	figures/tables/illustrations
Number of figures/tables/illustrations	4
Format	both print and electronic
Are you the author of this Elsevier article?	Yes
Will you be translating?	No
Order reference number	
Original figure numbers	Figure. 4.
Title of your thesis/dissertation	Effect of Void Fraction on Transverse Shear Modulus of Advanced Composites
Expected completion date	Jun 2016
Estimated size (number of pages)	90
Elsevier VAT number	GB 494 6272 12
Requestor Location	Jui-He Tai 10811 McKinley Dr. Apt. 12103, TAMPA, FL 33612 United States Attn: Jui-He Tai
Total	0.00 USD

Terms and Conditions

INTRODUCTION

1. The publisher for this copyrighted material is Elsevier. By clicking "accept" in connection with completing this licensing transaction, you agree that the following terms and conditions apply to this transaction (along with the Billing and Payment terms

https://s100.copyright.com/MyAccount/web/jsp/viewprintablelicensefrommyorders.jsp?ref=314483be-99bf-42f0-aef0-3125e34da5a4&email= 1/4

A.3 Permission from Minitab, Inc.

Figure 14, Figure 15, Figure 16, Figure 17, Figure 19, and Figure 20 are screenshots created with the software Minitab 15.

USF

Jui-He Tai <juihetai@mail.usf.edu>

Request for copyright permission to screenshots from Minitab 15

Minitab Inc Public Relations <publicrelations@minitab.com> Wed, Jun 15, 2016 at 9:22 AM
To: Jui-He Tai <juihetai@mail.usf.edu>

Hello!

Thank you for your request. Please accept this e-mail as permission to use the Minitab 15 graphs and figures for your thesis. As for referencing the graph, please see the information under "Screen Shots, Data sets, and Help Files" on our Author Permissions page; it should contain all the details you need.

http://www.minitab.com/en-us/author-permissions/

Best regards,

Eston

Eston Martz

Senior Creative Services Specialist

Minitab Inc.

Quality Plaza

1829 Pine Hall Road

State College, PA 16801 USA

814-753-3270

emartz@minitab.com

A.4 Permission from Taylor and Francis

Figure 3 is a copied figure from figure 4 in the book, “Phase Transformations in Metal and Alloys, Third Edition (Revised Reprint)” by David A. Porter, et al., which is published by Taylor and Francis Press.

Copyright Clearance Center

Confirmation Number: 11570053
Order Date: 06/14/2016

Customer Information

Customer: Jui-He Tai
Account Number: 3001036897
Organization: Jui-He Tai
Email: juihe.tai@gmail.com
Phone: +1 (813)8308682
Payment Method: Invoice

This is not an invoice

Order Details

Phase Transformations in Metals and Alloys, Third Edition (Revised Reprint)

Billing Status: **N/A**

Order detail ID:	69869683
ISBN:	9781439883570
Publication Type:	e-Book
Volume:	
Issue:	
Start page:	
Publisher:	Taylor and Francis
Author/Editor:	Porter, David A. ; Easterling, Kenneth E. ; Sherif, Mohamed

Permission Status: Granted
Permission type: Republish or display content
Type of use: Thesis/Dissertation
Order License Id: 3887950091666

Requestor type	Academic institution
Format	Print, Electronic
Portion	chart/graph/table/figure
Number of charts/graphs/tables/figures	1
Title or numeric reference of the portion(s)	Figure 4.2
Title of the article or chapter the portion is from	Chapter 4 - Solidification
Editor of portion(s)	N/A
Author of portion(s)	N/A
Volume of serial or monograph	N/A
Page range of portion	191
Publication date of portion	2009
Rights for	Main product
Duration of use	Life of current edition
Creation of copies for the disabled	no
With minor editing privileges	no
For distribution to	Worldwide
In the following language(s)	Original language of publication
With incidental promotional use	no

Lifetime unit quantity of new product	Up to 499
Made available in the following markets	education
The requesting person/organization	Jui-He Tai
Order reference number	
Author/Editor	Jui-He Tai
The standard identifier of New Work	Thesis Jui-He
Title of New Work	Effect of Void Fraction on Transverse Shear Modulus of Advanced Unidirectional Composites
Publisher of New Work	University of South Florida
Expected publication date	Aug 2016
Estimated size (pages)	80

Note: This item was invoiced separately through our **RightsLink service.** More info **$ 0.00**

ABOUT THE AUTHOR

Jui-He Tai was born in Taiwan in 1987 as the first of two sons from Yung-Ching Tai and Hsiang-Feng Wang. He obtained his Bachelor's degree in Earth Science from National Central University, Taoyuan City, Taiwan in June 2010. His senior undergraduate research project was on methane clathrate production and carbon dioxide sequestration. Furthermore, since he was certain about the transition to the field of materials upon graduation, he took some required materials-related undergraduate courses at National Tsing-Hua University, Hsinchu City, Taiwan in June 2013.

Jui-He Tai currently lives in Tampa, Florida. He is pursuing his Master degree in Material Science and Engineering at University of South Florida.

Before, studying abroad in the United States, he had two part-time work experiences in Taiwan. He worked as an electrician in Song Ling Co., Ltd Company in 2013, and as a part-time assistant in Nanyang Photocopy Shop in 2014. He also has a one-year mandatory military service experience.

In addition to taking courses at University of South Florida, he joined student organizations and participated in projects, such as Hybrid Motor High Powered Rocket Competition in March 2016 and NASA Student Launch Initiative in 2016 via USF Society of Aeronautics and Rocketry (SOAR), Electromagnetic Levitation project in 2016 via the Physics Club, and Coronary Angiography Design as an independent project in 2015 with Professor Venkat Bhethanabotla. Also, he passed the Fundamental of Engineering Exam (FE/EIT) administered by NCEES in January 2016.